AJP-Renal Physiol

Characterization of urinary exosomal release of aquaporin-1 and -2 after renal ischemia-reperfusion in rats

Siree Asvapromtada [1,4], Hiroko Sonoda[1,4], Minami Kinouchi[1,4], Sayaka Oshikawa[1], Saki Takahashi[1], Yuya Hoshino[1], Thitaporn Sinlapadeelerdkul[1], Naoko Yokota-Ikeda[2], Toshiyuki Matsuzaki[3], Masahiro Ikeda[1]

[1]Department of Veterinary Pharmacology, University of Miyazaki, Miyazaki 889-2192, Japan,
[2]Nephrology, Miyazaki Prefectural Miyazaki Hospital, and
[3]Department of Anatomy and Cell Biology, Gunma University Graduate School of Medicine
[4]These authors contributed equally to this work

Author contributions: H.S., M.K and M.I. designed the research; S.A., H.S., M.K., S.O., S.T., Y.H., T.S., N.I., T.M., and M.I. performed the research; S.A., H.S., M.K., T.M., and M.I. analyzed the data; S.A., H.S., M.K., T.M., and M.I. interpreted the results of experiments; S.A., H.S., T.M., and M.I. wrote the manuscript.

Running head: urinary exosomal release of AQPs in ischemic AKI

Contact information: Dr. Masahiro Ikeda, Department of Veterinary Pharmacology, Faculty of Agriculture, University of Miyazaki, Gakuenkibanadai-Nishi 1-1, Miyazaki 889-2192, Japan.
Phone: +81-985-58-7268; FAX: +81-985-58-7268;
E-mail: a0d302u@cc.miyazaki-u.ac.jp

ABSTRACT

Acute kidney injury (AKI) is an important risk factor for the development of chronic kidney disease (CKD) and an alteration in renal water handling has been observed during the transition of AKI to CKD. Urinary exosomal release of aquaporin-1 (AQP1) and AQP2, important proteins for renal water handling, has recently been reported to predict their levels of renal expression. We therefore examined the patterns of urinary exosomal release of AQP1 and AQP2, and the exosomal marker proteins tumor susceptibility 101 protein (TSG101) and ALG-2 interacting protein X (Alix), in the acute and chronic phases following induction of AKI by renal bilateral ischemia/reperfusion (I/R) in rats. Blood tests and histological examinations indicated that AKI occurred before at 7 days after renal I/R (day 7) and that renal fibrosis developed progressively thereafter. Immunoblotting demonstrated significant decreases in the urinary exosomal release of AQP1 and AQP2 during severe AKI. Urinary exosomal release of Alix and TSG101 was significantly increased on day 7. These data were also confirmed in rats with unilateral renal I/R causing more serious AKI. Urinary exosomal release of either the S256- or S269-phosphorylated form of AQP2, both of which are involved in apical trafficking of AQP2, was positively correlated with that of total AQP2. These results suggest that urinary exosomal release of AQP1 and AQP2 is reduced in I/R-induced AKI whereas that of Alix and TSG101 is increased in the initial phase of renal fibrosis. Furthermore, apical trafficking of AQP2 appears to be related to urinary exosomal release of AQP2.

Keywords: exosomes, extracellular vesicles, aquaporin-1, aquaporin-2, renal ischemia/reperfusion, tumor susceptibility 101 protein, ALG-2 interacting protein X, urine, renal fibrosis

INTRODUCTION

Acute kidney injury (AKI) is characterized by rapid reduction of the glomerular filtration rate (39). Chronic kidney disease (CKD) is a clinical syndrome characterized by a gradual decrease in kidney function over a period of months to a year, occasionally accompanied by renal interstitial fibrosis (14). Although these two syndromes were once thought to be separate diseases, epidemiologic and experimental studies in the past decade have indicated that they are mutually connected (14). For example, Coca et al. reported that AKI patients have a significantly higher risk of developing CKD than do patients without AKI (6). Therefore, the importance of the AKI-to-CKD transition has been increasingly recognized.

Exosomes, a specific subset of extracellular vesicles, originate from multivesicular bodies (MVBs). MVBs contain intraluminal vesicles which, after release into the extracellular space, are referred to as exosomes (7, 13, 22). The exosomes present in urine were first characterized by Pisitkun and colleagues in 2004 (37). They showed that exosomes were released into urine from all types of renal epithelial cells, including glomerular podocytes and renal tubule cells, and contained many types of membrane proteins related to renal function, such as aquaporins (AQPs), transporters, and ion-channels. Therefore, it has been proposed that urinary exosomes are a potential reservoir of biomarkers that reflect renal status (11, 19, 47). Also, our observations have shown that the levels of urinary exosomal AQP1 and AQP2 are related to the expression of these proteins in the kidney (1, 41).

AQPs are a class of integral membrane proteins, and at least seven isoforms (AQP1, AQP2, AQP3, AQP4, AQP6, AQP7, and AQP11) are known to be expressed in the kidney (20, 33, 42). Among them, AQP1 and AQP2 are well known to play important roles in renal water handling and both proteins have been found in urinary exosomes (1, 24, 34, 41, 44). AQP1 is expressed in the proximal tubule, the thin descending loop of Henle, and the descending vasa recta. Previous functional analyses have revealed that AQP1 plays important roles in tubule water permeability and the mechanisms of counter-current exchange in the kidney (20, 33, 42). AQP2 is a vasopressin-regulated water channel. When the type 2 receptor for vasopressin (V2 receptor) in the principal cells of the renal collecting duct is activated by vasopressin binding, AQP2 is rapidly translocated from intracellular vesicles to the apical membrane, resulting in an acute increase of water reabsorption. In addition to this acute response, activation of the V2 receptor increases the expression of AQP2 protein in the principal cells through enhanced transcription, contributing to chronic regulation of water

reabsorption by vasopressin (20, 33, 42).

Renal ischemia/reperfusion (I/R) injury is a major cause of AKI (21). So far, mice and rats subjected to renal I/R have been used exclusively as models of AKI. Since rodent renal I/R has also been reported to cause renal fibrosis after severe AKI, some studies have used these animals as models of renal fibrosis (4, 9, 12, 35). Interestingly, Basile et al. (4) observed that in rats renal I/R led to a significant urinary concentration defect over a period of months. Because this disturbance of renal water handling has also been seen in human CKD (36), the rodent I/R model is thought to be an appropriate one for the AKI-CKD (renal fibrosis) transition accompanied by alteration of renal water handling. However, it is still largely unknown whether the release of urinary exosomal AQP1 and AQP2 is altered during the AKI-to-CKD transition phase in rodent I/R models.

In order to characterize the release pattern of urinary exosomal AQP1 and AQP2 in the acute and chronic phases after renal I/R, possibly leading to a means of assessing the state of renal water handling, we employed a rat model of renal I/R and examined the levels of urinary exosomal release and renal expression of AQP1 and AQP2. We also examined the pattern of exosomal release of marker proteins, including tumor susceptibility gene 101 protein (TSG101) and ALG-2 interacting protein X (Alix) (11, 34). Moreover, we measured the urinary exosomal release of the S256- and S269-phosphorylated forms of AQP2, both of which are related to trafficking of AQP2 to the apical membrane (23).

MATERIALS AND METHODS

Animal models, and blood and urine analyses.

All animal studies were conducted with approval from the University of Miyazaki in accordance with the University Guidelines for Institutional Care and Use of Laboratory Animals. Male Sprague-Dawley (SD) rats aged 10 weeks were purchased from Kyudo (Saga, Japan). All the animals had free access to water and a normal diet. The rats were randomly divided into two groups: a control group subjected to a sham operation and a group subjected to an I/R operation. In the operation to induce bilateral renal I/R (B-I/R), the left and right renal vascular pedicles were occluded using two microvascular clamps (Roboz, Gaithersburg, MD) for 25 minutes, and then the kidneys were reperfused with blood (21). The sham operation involved an identical surgical procedure without clamping of the renal pedicles. The day of the operation for I/R was designated as day 0. Blood and urine samples were collected on day 3 (sham, n = 15; I/R, n = 19; from 3 experiments), day 7 (sham, n = 11; I/R, n = 14; from 2 experiments), day 21 (sham, n = 5; I/R, n = 7; from 1 experiment), and day 35 (sham, n = 5; I/R, n = 7; from 1 experiment). During urine collection, all animals were kept in metabolic cages and given free access to water. Kidney samples were obtained on day 3 (sham, n = 4; I/R, n = 5), day 7 (sham, n = 6; I/R, n = 7), and day 35 (sham, n = 5; I/R, n = 7).

For the operation to induce renal unilateral I/R (U-I/R), the following procedures were performed. One week after removal of the right kidney, the left renal vascular pedicle was occluded using two microvascular clamps for 35 minutes and then the kidney was reperfused with blood. The sham operation for U-I/R involved an identical surgical procedure without clamping of the renal pedicle. Blood samples were collected on day 3 (sham, n = 8; I/R, n = 8; from 2 experiments), day 7 (sham, n = 8; I/R, n = 8; from 2 experiments), and day 35 (sham, n = 4; I/R, n = 4; from 1 experiment). Urine samples were collected on day 7 (sham, n = 4; I/R, n = 4; from 1 experiment) and day 35 (sham, n = 4; I/R, n = 4; from 1 experiment). Kidney samples were obtained on day 7 (sham, n = 4; I/R, n = 4), and day 35 (sham, n = 4; I/R, n = 4).

The plasma urea nitrogen and creatinine concentrations were measured using an autoanalyzer (Fuji Film Medical, Tokyo, Japan) and urine osmolality was measured using an automatic osmometer (Arkray, Inc., Kyoto, Japan).

Isolation of urinary exosomes.

Isolation of a urinary exosome-rich fraction was performed by sequential centrifugation as described previously (15, 41). In brief, urine collected for 6 h from each rat was centrifuged immediately after collection at 1,000 × g for 15 min, and the supernatant was centrifuged at 17,000 × g for 15 min. The resulting supernatant was retained, and the pellet was incubated at 37°C with a DTT (50 mg/ml) -containing isolation solution (250 mM sucrose, 10 mM triethanolamine, 8 mM Hepes, pH 7.6). After incubation, the pellet suspension was centrifuged at 17,000 × g for 15 min. The supernatants from the first and second centrifugations were combined, and the mixed solution was ultracentrifuged at 200,000 × g for 1 h (Optima TL Ultracentrifuge; Beckman Instruments, CA). The resulting pellet was solubilized with water containing a protease inhibitor, and this suspension was mixed with 4 × sample buffer (8% SDS, 50% glycerol, 250 mM Tris-Cl, 0.05% bromophenol blue, 200 mM DTT, pH 6.8). These samples were stored at -80°C. Each urinary exosomal protein sample was loaded with the same amount of urinary creatinine for immunoblot analysis.

Renal protein extraction.

The cortex and medulla of the kidney from each rat was homogenized for 5 min at 4°C using a shaker-type homogenizer (BioMedical Science Inc., Tokyo, Japan). The homogenate was centrifuged at 1,000 × g for 10 min at 4°C and the supernatant was then centrifuged at 200,000 × g for 1 h at 4°C. The resulting 1,000 × g supernatant (for detection of renal β-actin) and 200,000 × g pellet (for detection of renal AQP1 and AQP2) were separately dissolved in an isolation solution, followed by mixing with 4 × sample buffer, and incubated for 30 min at 37°C. For immunoblot analysis, each renal protein sample was loaded with the same amount of total protein.

Immunoblot analysis.

Immunoblot analysis was performed as described previously (15, 41) using the following antibodies: anti-AQP1 (cat no. sc20810; Santa Cruz Biotechnology Inc., Santa Cruz, CA), rabbit anti-AQP2 (cat no. AQP-002; Alomone Labs, Jerusalem, Israel), goat anti-AQP2 (cat no. sc-9882, Santa Cruz Biotechnology, Santa Cruz, CA), anti-TSG101 (cat no. ab-125011; Abcam Inc., MA, USA), anti-Alix (cat no. sc-49268; Santa Cruz Biotechnology Inc.), anti-S256-phosphorylated AQP2 (house-made antibody), anti-S269-phosphorylated AQP2 (house-made antibody) (40)(Fig. 11), anti-β-actin (cat no. sc-4778; Santa Cruz Biotechnology Inc.), anti-mouse IgG (cat no. 1858413; Thermo Fisher Scientific Inc., Rockford, IL), anti-rabbit

IgG (cat no. 7074; Cell Signaling Technology, Danvers, MA), anti-goat IgG (cat no. P0449; Dako Japan, Tokyo, Japan), Rhodamine Red-X-conjugated donkey anti-rabbit IgG (cat no. 711-295-152, Jackson Immunoresearch, West Grove, PA), and Alexa Fluor 488-conjugated donkey anti-goat IgG (cat no. A11055, Life Technologies, Grand Island, NY).

We had previously confirmed the specificities of anti-S256-phosphorylated and anti-S269-phosphorylated AQP2 by immunofluorescence using absorption of the peptide as an immunogen and phosphatase-treated samples (40)(Fig. 11). To generate the anti-S256-phosphorylated AQP2 antibody, a partial peptide corresponding to amino acids 254–258 of rat AQP2 (i.e., RQSVE) was chosen as the immunogen. Synthetic oligopeptides phosphorylated or non-phosphorylated at S256 (named TM61 and TM64, respectively), to which cysteine residues were added at their N-termini, were obtained from Operon Biotechnology (Tokyo, Japan). The rabbit polyclonal antibody against S256-phosphorylated AQP2 was developed using the TM61 oligopeptide that was conjugated to keyhole limpet hemocyanin using an Imject maleimide-activated mcKLH kit (77611, Thermo Scientific, Rockford, IL). To obtain the specific antibody, affinity purification was performed as follows. Serum was applied to a TM64-coupled agarose column gel (Sulfolink coupling resin; 20401, Thermo Scientific) to completely absorb the antibody to the non-phosphorylated form, and the serum that passed through was collected. The absorbed serum was then applied to a TM61-coupled agarose gel column, and the specific antibody was eluted and dialyzed using phosphate-buffered saline (PBS).

The resulting bands were visualized using the SuperSignal West-Femto Chemiluminescence detection system (Thermo Fisher Scientific, Waltham, MA) and quantified using ImageQuant TL software (GE Healthcare, Uppsala, Sweden).

Histology.

The kidney samples were embedded in paraffin blocks, cut into sections 2 μm thick, and then subjected to Masson's trichrome staining. For immunohistochemistry, the sections were deparaffinized and rehydrated, and the antigens were retrieved by incubating each specimen in distilled water at 121°C for 5 min. Each slide was then incubated with primary antibodies against AQP1, AQP2, and α-smooth muscle actin (α-SMA) at 37 °C for 1 h followed by incubation with Envision System Labelled Polymer Reagent (Dako Japan) at 37 °C for 45 min. The reaction product was visualized by treatment with 3, 3'-diaminobenzidine

tetrahydrochloride, and the specimen was counterstained with hematoxylin.

Statistical analysis.

All quantitative data are presented as means ± SE. Statistical comparisons between the sham and I/R groups were analyzed by Mann-Whitney U test (fewer than 10 samples, or more than 10 samples when there was a significant difference in the distribution and homogeneity of variance between the groups as judged by the Shapiro–Wilk test and F test, respectively) or Student's t-test (more than 10 samples when there was no significant difference in the distribution and homogeneity of variance between the groups), and differences at $P < 0.05$ were considered to be statistically significant. For investigation of linear relationships between two quantitative variables, Pearson's correlation coefficient was calculated.

RESULTS

Changes in plasma and urinary parameters after renal B-I/R.

Figure 1 shows the changes in plasma urea and creatinine concentrations, urine volume, and urinary osmolality after renal B-I/R. Plasma concentrations of creatinine and urea nitrogen on day 3 were dramatically increased about 11- and 8-fold relative to the sham group, respectively. Thereafter, these concentrations in the B-I/R group decreased, and by days 21 and 35 they showed no obvious difference from those in the sham group. As shown in Fig. 1C, there was no significant inter-group difference in urine volume at any of the time points examined. The urinary osmolality on day 3 was significantly decreased in the B-I/R group relative to the sham group (Fig. 1D). These data confirmed that our surgical procedure caused B-I/R-induced AKI, accompanied by an initial urinary concentration defect.

Development of renal fibrosis in rat B-I/R kidney.

Renal histology was assessed by either Masson's trichrome staining for detection of collagen fibers or immunohistochemistry for α-SMA (Fig. 2), a marker protein for myofibroblasts. Renal collagen fibers were clearly observed in the renal interstitium on day 7 and beyond (Fig. 2, A - D). On the other hand, renal α-SMA was apparently expressed on day 3 and beyond, and peaked on day 7 (Fig. 2, E - I), mainly in the renal interstitium. These data indicated that renal fibrosis developed after renal B-I/R, being initially marked in myofibroblasts (peaking on day 7), followed by deposition of collagen fibers in the renal interstitium.

Urinary exosomal release of AQP1, AQP2, and exosomal marker proteins after renal B-I/R.

We examined whether urinary exosomal release of AQP1 and AQP2 was altered after renal B-I/R. Figures 3A and B show examples of immunoblotting for exosomal AQP1 and a summary of the data, respectively. As shown in Fig. 3A, two bands were detected by immunoblotting, the upper band representing glycosylated AQP1 and the lower band non-glycosylated AQP1 (41). Exosomal release of glycosylated, non-glycosylated, and combined AQP1 after renal B-I/R was significantly decreased on days 3 and 7, the reduction being greater on day 3.

Figure 4 shows data for exosomal release of AQP2. As observed for AQP1, both glycosylated and non-glycosylated AQP2 was detected (15). Exosomal release of both forms of AQP2 after renal B-I/R was significantly decreased on day 3, and then recovered to a level comparable to that in the sham group on day 7. Interestingly, on days 21 and 35, the levels again

tended to be decreased.

Since it has been considered that Alix and TSG101 are marker proteins for exosomes (11, 34), we examined whether alterations in the exosomal release of AQPs were attributable to a change in the number of exosomes released into urine after renal B-I/R by measuring exosomal release of the marker proteins Alix and TSG101. Unexpectedly, as shown in Fig. 5, urinary exosomal release of Alix was significantly increased by renal B-I/R on day 7. Similarly, renal I/R significantly increased the urinary exosomal release of TSG101 (Fig. 6) on days 7 and 21, and the level peaked on day 7.

Renal expression levels of AQP1 and AQP2 after renal B-I/R.

Next, we examined the levels of renal expression of AQP1 and AQP2 on days 3, 7, and 35. All quantitative data were normalized relative to β-actin as an internal control. As shown in Fig. 7, the expression level of renal cortical AQP1 was significantly reduced by renal B-I/R on day 3, whereas on day 35 the level tended to be increased. On the other hand, the level of AQP1 expression in the medulla was decreased by renal B-I/R at all time points, being prominent at earlier time points when the events of AKI were ongoing (days 3 and 7).

Figure 8 shows the data for renal expression of AQP2. In the cortex, on days 3 and 35, the levels of AQP2 expression were clearly decreased in the B-I/R group relative to the sham group. However, the cortical expression level of AQP2 was not markedly reduced on day 7. In the medulla, the level of AQP2 was significantly decreased at all time points, the reduction being greater on days 3 and 7 than on day 35.

Renal immunohistochemistry for AQP1 and AQP2.

Figures 9 and 10 show the results of immunohistochemistry for AQP1 (Fig. 9) and AQP2 (Fig. 10) on days 3, 7, and 35. As shown in Fig. 9, relative to the sham group, AQP1-positive cells in the cortex were obviously reduced with dilatation of the tubules on day 3 in the B-I/R group. The level of expression gradually recovered on days 7 and 35, thus corroborating the results of immunoblotting (Fig. 7C). In the medulla, patterns similar to those obtained in the cortex were observed (data not shown).

In the cortex on days 3 and 35, AQP2-positive cells were reduced in the B-I/R group in comparison with the sham group, thus corroborating the results of immunoblotting (data not shown). On the other hand, on day 7, the B-I/R group showed no marked changes in the number

of AQP2-positive cells or the subcellular localization of AQP2 in comparison with the sham group (data not shown). In the medulla on day 3 (Fig. 10, A-D), renal B-I/R reduced the number of AQP2-positive cells although the subcellular localization of AQP2 expression did not differ markedly from that in the sham group, being mainly intracellular. By day 7, the number of AQP2-positive cells had recovered somewhat. Interestingly, on day 7, AQP2 was clearly expressed in the both apical and basolateral membrane in the I/R group (Fig. 10 G). On day 35, the number of AQP2-positive cells was higher than that on day 3 in the I/R group, and basolateral localization of AQP2 was not observed.

Phosphorylated forms of AQP2 in urinary exosomes.

It has been suggested that phosphorylation of Ser256 in AQP2 is involved in the trafficking of AQP2 from intracellular vesicles to the surface membrane (23). Therefore, we examined the S256-phosphorylated form of AQP2 in urinary exosomes after renal B-I/R. For this purpose, the specificity of the anti-S256-phosphorylated AQP2 antibody was initially verified by immunofluorescence. As shown in Fig. 11, the anti-S256-phosphorylated AQP2 antibody intensely labeled the collecting duct cells in the kidney slice from AVP-administered rat (Fig. 11 A). This labeling was abolished by addition of the Ser256-phosphorylated peptide (TM61) (Fig. 11B), but not by addition of the non-phosphorylated peptide (TM64) (Fig. 11C). We further demonstrated that the labeling completely disappeared when the kidney slice was treated with lambda protein phosphatase (Fig. 11 F). These results confirmed that the anti-S256-phosphorylated AQP2 antibody specifically detected the S256-phosphorylated form of AQP2.

As shown in Fig. 12, A and B, the S256-phosphorylated form of glycosylated and non-glycosylated AQP2 was clearly detectable in the urinary exosomal fraction, and the pattern of exosomal release after renal B-I/R resembled that of total (phosphorylated + non-phosphorylated) AQP2 (Fig. 4B). Therefore, we evaluated the relationship between urinary exosomal release of total AQP2 and the S-256-phosphorylated form of AQP2. As shown in Fig. 12C, there was a significant positive correlation between them.

As it has been reported that phosphorylation of Ser269 is involved in the apical membrane retention of AQP2 (23), we also examined the S269-phosphorylated form of AQP2 in urinary exosomes after renal I/R. The specificity of the antibody used in this experiment has been verified (40). As shown in Fig.13A, we detected the S269-phosphorylated form of

non-glycosylated AQP2 in urinary exosomes, but the band intensity was weaker than those of total AQP2 and the S256-phosphorylated form of AQP2. For glycosylated AQP2, the band intensity was too weak to allow quantification of the data (data not shown), and therefore we quantified only the S269-phosphorylated form of non-glycosylated AQP2. Renal B-I/R tended to decrease the urinary exosomal release of S269-phosphorylated AQP2 on days 3 and 35 (Fig. 13). On the other hand, the release was high on day 7 and was not altered on day 21 in comparison with the sham group. Figure 13C shows the relationship between urinary exosomal total AQP2 and the S-269-phosphorylated form of AQP2. A significant positive correlation was evident, and the correlation coefficient was lower than for the S-256-phosphorylated form of AQP2.

Changes in plasma and urinary parameters after renal U- I/R.

Basile et al. (4) observed that I/R led to a significant decrease of urine osmolality and volume until 40 days after renal I/R. In contrast, we observed a decrease of urinary osmolality only on day 3 as described earlier (Fig. 1 C). Although the reason for this difference is still unclear, it may have been related to the difference in the severity of AKI. Therefore we employed a U-I/R model (contralateral nephrectomy).

Table 1 shows the changes in plasma urea and creatinine concentrations, urine volume, and urinary osmolality after renal U-I/R. Plasma concentrations of urea nitrogen and creatinine on days 3 and 7 were significantly increased in the U-I/R group in comparison with the sham group. The levels were also higher than those in the B-I/R group, suggesting that U-I/R caused more severe AKI. The urinary osmolality on day 7 was significantly decreased in the U-I/R group relative to the sham group and tended to be decreased on day 35. Furthermore, the urinary volume on days 7 and 35 was significantly increased in the U-I/R group relative to the sham group. These data indicated that U-I/R-induced a more severe urinary concentrating defect.

Renal histology in U-I/R kidney.

Renal histology was assessed after U-I/R using either Masson's trichrome staining or immunohistochemistry for α-SMA (Fig. 14, A-F). Renal collagen fibers were clearly observed in the renal interstitium on day 7 and beyond (Fig. 14, A - C). Renal α-SMA was also apparently expressed on day 7 and beyond (Fig. 14, D - F), the increase being greater on day 7 (Fig. 2, E - I). These findings were in good agreement with the B-I/R data.

Figures, 14 G - L show the results of immunohistochemistry for AQP1 (Fig. 14, G - I) and AQP2 (Fig. 14, J - L) on days 7 and 35. As shown in Fig. 14 H, relative to the sham group, AQP1-positive cells in the cortex were markedly reduced with dilatation of the tubules on day 7 in the U-I/R group. The level of expression had recovered somewhat by day 35, but still remained low. For AQP2, on day 7, positive cells in the U-I/R group were reduced in comparison with the sham group and, in contrast to the results obtained by B-I/R, AQP2 was clearly expressed only in the apical membrane in the U-I/R group (black box in Fig. 14 K). On day 35, renal U-I/R led to a decrease in the expression of AQP2, although its subcellular localization did not differ markedly from that in the sham group.

Urinary exosomal release of proteins after renal U-I/R.

We examined whether urinary exosomal release of AQP1, AQP2, Alix and TSG101 was altered after renal U-I/R. Figure 15, A and B show examples of immunoblotting for exosomal AQP1 and a summary of the data, respectively. Exosomal release of glycosylated, non-glycosylated, and combined AQP1 after renal U-I/R was significantly decreased on day 7 and this reduction was greater than that after renal B-I/R (Fig. 3).

Figures 15 C and D show data for exosomal release of AQP2. Exosomal release of both glycosylated and non-glycosyloated AQP2 after renal U-I/R was significantly decreased on day 7, and tended to be decreased on day 35. These reductions were greater in comparison with renal B-I/R.

As shown in Figs. 15 E - H, urinary exosomal release of Alix and TSG101 was significantly increased by renal U-I/R on day 7. On day 35, the increases were still evident but did not reach significant levels in comparison with the sham group.

DISCUSSION

The purpose of this study was to determine the pattern of exosomal release of AQP1 and AQP2 during the progression of AKI to renal fibrosis using rats subjected to renal B- or U- I/R. To this end, the models we used in this study were thought to be appropriate. Plasma urea nitrogen and creatinine concentrations were markedly increased on day 3, and decreased thereafter. Histological analyses showed that α-SMA was maximally expressed on day 7. Renal tubulointerstitial collagen fibers, demonstrated by Masson's trichrome staining, increased progressively after day 7. These observations showed that AKI occurred at an early stage (before day 7), and that the initial events of renal fibrosis were evident around day 7, the fibrosis increasing progressively thereafter in both I/R models. This time course of renal I/R-induced injury was in accord with several reports of observations using similar experimental models (4, 9, 12, 28, 35).

During the transition of AKI to renal fibrosis, the pattern of urinary release of exosomal AQP1 and AQP2 we observed was as follows. Reduced urinary exosomal release of AQP1 and AQP2 in the B-I/R group, a milder AKI model, was observed on day 3 but not on day 7. In contrast, when we used the U-I/R model, which causes more serious AKI, significant decreases in the urinary exosomal release of AQP1 and AQP2 were observed on day 7. Thereafter , urinary exosomal release of AQP2, but not AQP1, tended to be reduced, and this lower level was maintained until day 35 in both models, the decrease being greater in the U-I/R model, which exhibited a significant increase in urinary volume and a tendency for a decrease in urinary concentration. Therefore, these results suggest that in the AKI phase, the abundance of AQP1 and AQP2 in urinary exosomes might be decreased, corroborating our previous data for AQP1 (41). Furthermore, urinary exosomal release of AQP2 might be decreased during the period when renal fibrosis is developing, accompanied by a urinary concentration defect.

Urinary exosomal release of both Alix and TSG101 was unchanged on day 3 and significantly increased on day 7 in the B-I/R group, accompanied by marked renal expression of α-SMA, suggesting onset of renal fibrosis. These increases for Alix and TSG101 were also confirmed using the U-I/R model. Since both proteins are thought to be markers of exosomes (11, 34), the increase in Alix and TSG101 strongly suggested that the total number of exosomes released into urine on day 7 was increased in our I/R models. Taking into account the maximum expression of α-SMA on day 7, Alix and TSG101 released in urinary exosomes might be applicable as biomarkers for detection of renal fibrosis onset.

It has been reported that exosomal release is increased under hypoxic conditions (27, 38). Furthermore, King et al. have clearly shown that hypoxic enhancement of exosome release by breast cancer cells is prevented by treatment with siRNA against hypoxia-inducible factor 1α (HIF1α) (26), suggesting that the hypoxia-induced increase in the number of exosomes released is mediated by the HIF1α pathway. On the other hand, Conde et al. (8) have demonstrated that HIF1α is markedly expressed in the kidney 5 days after renal I/R. These findings suggest that enhanced expression of HIF1α after renal I/R increased the number of exosomes released into urine, thus accounting for the increased levels of Alix and TSG101 detected on day 7 in the present study.

The reduced urinary exosomal release of AQP1 in the B-I/R group was accompanied by a decrease in its renal expression on days 3 (in the cortex and medulla) and 7 (in the medulla and decreasing tendency in the cortex). Therefore, on day 3, the markedly reduced exosomal release of AQP1 in the B-I/R group might have been attributable to a decrease in the cortical and medullary expression of AQP1. Furthermore, on day 7, despite an increase in the number of exosomes, reduced expression of AQP1 in the medulla and a tendency for a decrease in the cortex may have led to a net decrease in the urinary exosomal release of AQP1 at this time point.

After renal B-I/R, renal cortical expression of AQP2 was decreased on days 3 and 35, and its medullary expression was decreased throughout the observation period. The reduction of AQP2 expression in the medulla was greater on days 3 and 7 than on day 35. It has been shown that the expression level of AQP2 in the renal medulla evaluated by immunoblotting is considerably higher than in the cortex (37). On the other hand, as mentioned earlier, the number of exosomes released into urine might be increased only on day 7. Taken together, these observations suggest that the urinary exosomal release of AQP2 on day 3 was attributable to lower levels of renal medullary expression without any change in the number of exosomes released into urine. On day 7, an increase in the number of exosomes masked the lower abundance of medullary AQP2 expression, leading to unaltered urinary exosomal release of AQP2. On day 35, the level of urinary exosomal AQP2 release was attributable to a mild decrease in the level of renal medullary AQP2 expression without any change in the number of exosomes released into urine. However, the mechanisms regulating the urinary release of both AQP2 and AQP1 are still poorly understood, and therefore the factors determining the level at which they are released into urine after renal I/R await further investigation.

Although AQP2 is well known to be a functional protein at the apical membrane, as shown in Fig. 10, renal B-I/R caused clear basolateral localization of AQP2 on day 7. On the other hand, in the U-I/R model, basolateral localization of AQP2 disappeared. The reason for this discrepancy was not clear. Several previous studies have shown that although AQP2 is a functional protein at the apical membrane, it is expressed basolaterally in collecting duct cells, and several mechanisms for this basolateral expression have been proposed, including roles for hypertonicity (43), aldosterone (10), vasopressin (10), blockade of endocytosis (46), and integrin-β1 (5), which is a binding protein for AQP2. Therefore, it is conceivable that some of these mechanisms may be involved in the differences we observed between the two models. It has been pointed out that basolateral expression of AQP2 may play a novel role in cell migration and epithelial morphogenesis, which are unlikely to be dependent on its water transport function (5). Therefore, the mechanisms responsible for the basolateral expression of AQP2 after renal B-I/R remain to be clarified in future studies.

In the present study, we examined urinary exosomal release of either the S256- or S269- phosphorylated form of AQP2 after renal B-/R. Phosphorylation has been shown to play critical roles in the subcellular localization of AQP2 (20, 23). The COOH-terminal region of the AQP2 molecule has four serine residues (Ser256, Ser261, Ser264, and Ser269) that are known to be targets for phosphorylation regulation (16, 17, 20, 23). Among them, the most extensively studied phosphorylation site is Ser256 (20). The S256-phosphorylated form of AQP2 has been observed at the plasma membrane and in intracellular vesicles. Although vasopressin fails to phosphorylate Ser256 in AQP2, studies employing a substitution-mutation at Ser256 in AQP2, which prevents phosphorylation of this site, have shown that basal phosphorylation of Ser256 is important for vasopressin-induced translocation of AQP2 from intracellular vesicles to the apical membrane (25, 30). In contrast to the unresponsiveness of Ser256 to vasopressin, the level of phosphorylation at Ser269 in AQP2 is known to increase dramatically in response to vasopressin (45). It has also been shown that phosphorylation at Ser269 may be involved in retention of AQP2 at the apical membrane through a mechanism that prevents endocytosis. This inhibition of endocytosis is thought to be mediated by inhibition of polyubiquitination at Lys270, which is located next to Ser269 (32). Interestingly, phosphorylation of Ser269 has been reported to depend on prior phosphorylation at Ser256 (16). Collectively, it is conceivable that basal phosphorylation of Ser256 is important for exocytosis of AQP2 in spite of its poor sensitivity to vasopressin, and that phosphorylation of Ser269 prevents endocytosis of AQP2 in a

vasopressin-dependent manner, both being involved in the apical membrane expression of AQP2. In the present study, the level of either of the phosphorylated forms of AQP2 in exosomes was positively correlated with that of total AQP2 in urinary exosomes. These data suggest that exosomal release of AQP2 into urine is related to the apical membrane expression of AQP2. However, according to the best-described mechanism for genesis of exosomes, the exosomal release of membrane proteins is thought to be dependent on their endocytosis (7, 13), and therefore detection of the S269- phosphorylated form of AQP2 appears to be unexpected. Although any explanation seems uncertain at present, we cannot completely exclude the possibility that a small portion of vesicles that had been produced by outward budding and fission of the plasma membrane may have contaminated our exosomal fraction, leading to the detection of S269- phosphorylated AQP2. However, this seems unlikely because the exosomal fraction was obtained by ultra-centrifugation and clearly contained exosomal marker proteins. Also, in a preliminary experiment, Nanosight analysis showed that the size distribution of membrane-bound vesicles in our exosomal fraction had a mode of around 70 nm and a standard deviation of around 50 nm, suggesting that the fraction was rich in exosomes (<100 nm in diameter) with only a minimal amount of contaminating budding vesicles with a larger diameter (>200 nm) (7). Although it had been thought that ubiquitin is cleaved from ubiquitinated cargo protein during exosome genesis (2, 3, 29, 31), ubiquitinated AQP2 has recently been observed in human urinary exosomes (18), suggesting that the proposed pathway for exosome genesis may need to be reevaluated.

Recent epidemiological and experimental observations have shown that AKI contributes to the development and progression of CKD, suggesting the importance of the AKI-CKD transition (14). Currently in clinical practice, it is difficult to detect the state of the AKI-CKD transition. Therefore, the discovery of potential non-invasive biomarkers that reflect each stage of AKI-CKD transition would be highly desirable. We anticipate that our present findings will lead to the development of a method for clinical monitoring of a combination of urinary exosomal proteins, which would be useful for detecting the transition of AKI to renal fibrosis.

FUNDING

The work is supported by JSPS KAKENHI, 25660241 (M.I.), 25221205 (M.I.), 15H04594 (M.I.), 16K15047 (M.I.), 24780287 (H.S.), and 15K18784 (H.S.).

CONFLICT OF INTEREST STATEMENT

None declared.

REFERENCES

1. **Abdeen A, Sonoda H, El-Shawarby R, Takahashi S, Ikeda M.** Urinary excretion pattern of exosomal aquaporin-2 in rats that received gentamicin. *Am J Physiol Renal Physiol* 307: F1227-F1237, 2014.

2. **Agromayor M, Martin-Serrano J.** Interaction of AMSH with ESCRT-III and deubiquitination of endosomal cargo. *J Biol Chem* 281: 23083-23091, 2006.

3. **Amerik AY, Nowak J, Swaminathan S, Hochstrasser M.** The Doa4 deubiquitinating enzyme is functionally linked to the vacuolar protein-sorting and endocytic pathways. *Mol Biol Cell* 11: 3365-3380, 2000.

4. **Basile DP, Donohoe D, Roethe K, Osborn JL.** Renal ischemic injury results in permanent damage to peritubular capillaries and influences long-term function. *Am J Physiol Renal Physiol* 281: F887-F899, 2001.

5. **Chen Y, Rice W, Gu Z, Li J, Huang J, Brenner MB, Van Hoek A, Xiong J, Gundersen GG, Norman JC, Hsu VW, Fenton RA, Brown D, Lu HA.** Aquaporin 2 promotes cell migration and epithelial morphogenesis. *J Am Soc Nephrol* 23: 1506-1517, 2012.

6. **Coca SG, Singanamala S, Parikh CR.** Chronic kidney disease after acute kidney injury: a systematic review and meta-analysis. *Kidney Int* 81: 442-448, 2012.

7. **Colombo M, Raposo G, Théry C.** Biogenesis, secretion, and intercellular interactions of exosomes and other extracellular vesicles. *Annu Rev Cell Dev Biol* 30: 255–289, 2014.

8. **Conde E, Alegre L, Blanco-Sánchez I, Sáenz-Morales D, Aguado-Fraile E, Ponte B, Ramos E, Sáiz A, Jiménez C, Ordoñez A, López-Cabrera M, del Peso L, de Landázuri MO, Liaño F, Selgas R, Sanchez-Tomero JA, García-Bermejo ML.** Hypoxia inducible factor 1-alpha (HIF-1 alpha) is induced during reperfusion after renal ischemia and is critical for proximal tubule cell survival. *PLoS One* 7: e33258, 2012.

9. **Cruzado JM, Torras J, Riera M, Herrero I, Hueso M, Espinosa L, Condom E, Lloberas N, Bover J, Alsina J, Grinyó JM.** Influence of nephron mass in development of chronic renal failure after prolonged warm renal ischemia. *Am J Physiol Renal Physiol* 279: F259-F269, 2000.

10. **de Seigneux S, Nielsen J, Olesen ET, Dimke H, Kwon TH, Frøkiaer J, Nielsen S.** Long-term aldosterone treatment induces decreased apical but increased basolateral expression of AQP2 in CCD of rat kidney. *Am J Physiol Renal Physiol* 293: F87-F99, 2007.

11. **Erdbrügger U, Le TH**. Extracellular vesicles in renal diseases: more than novel

biomarkers? *J Am Soc Nephrol* 27: 12-26, 2016.

12. **Forbes JM, Hewitson TD, Becker GJ, Jones CL.** Ischemic acute renal failure: long-term histology of cell and matrix changes in the rat. *Kidney Int* 57: 2375-2385, 2000.

13. **Hanson PI, Cashikar A.** Multivesicular body morphogenesis. *Annu Rev Cell Dev Biol* 28: 337-362, 2012.

14. **He L, Wei Q, Liu J, Yi M, Liu Y, Liu H, Sun L, Peng Y, Liu F, Venkatachalam MA, Dong Z.** AKI on CKD: heightened injury, suppressed repair, and the underlying mechanisms. *Kidney Int* 92: 1071-1083, 2017.

15. **Higashijima Y, Sonoda H, Takahashi S, Kondo H, Shigemura K, Ikeda M.** Excretion of urinary exosomal AQP2 in rats is regulated by vasopressin and urinary pH. *Am J Physiol Renal Physiol* 305: F1412-F1421, 2013.

16. **Hoffert JD, Fenton RA, Moeller HB, Simons B, Tchapyjnikov D, McDill BW, Yu MJ, Pisitkun T, Chen F, Knepper MA.** Vasopressin-stimulated increase in phosphorylation at Ser269 potentiates plasma membrane retention of aquaporin-2. *J Biol Chem* 283: 24617-24627, 2008.

17. **Hoffert JD, Pisitkun T, Wang G, Shen RF, Knepper MA.** Quantitative phosphoproteomics of vasopressin-sensitive renal cells: regulation of aquaporin-2 phosphorylation at two sites. *Proc Natl Acad Sci U S A* 103: 7159-7164, 2006.

18. **Huebner AR, Cheng L, Somparn P, Knepper MA, Fenton RA, Pisitkun T.** Deubiquitylation of protein cargo is not an essential step in exosome formation. *Mol Cell Proteomics* 15: 1556-1571, 2016.

19. **Huebner AR, Somparn P, Benjachat T, Leelahavanichkul A, Avihingsanon Y, Fenton RA, Pisitkun T.** Exosomes in urine biomarker discovery. *Adv Exp Med Biol* 845: 43-58, 2015.

20. **Ikeda M, Matsuzaki T.** Regulation of aquaporins by vasopressin in the kidney. *Vitam Horm* 98: 307-337, 2015.

21. **Ikeda M, Prachasilchai W, Burne-Taney MJ, Rabb H, Yokota-Ikeda N.** Ischemic acute tubular necrosis models and drug discovery: a focus on cellular inflammation. *Drug Discov Today* 11: 364-370, 2006.

22. **Johnstone RM, Adam M, Hammond JR, Orr L, Turbide C.** Vesicle formation during reticulocyte maturation. Association of plasma membrane activities with released vesicles (exosomes). *J Biol Chem* 262: 9412–9420, 1987.

23. **Jung HJ, Kwon TH.** Molecular mechanisms regulating aquaporin-2 in kidney collecting duct. *Am J Physiol Renal Physiol* 311: F1318-F1328, 2016.

24. **Kanno K, Sasaki S, Hirata Y, Ishikawa S, Fushimi K, Nakanishi S, Bichet DG, Marumo F.** Urinary excretion of aquaporin-2 in patients with diabetes insipidus. *N Engl J Med* 332: 1540-1545, 1995.

25. **Katsura T, Gustafson CE, Ausiello DA, Brown D.** Protein kinase A phosphorylation is involved in regulated exocytosis of aquaporin-2 in transfected LLC-PK1 cells. *Am J Physiol* 272: F817-F822, 1997.

26. **King HW, Michael MZ, Gleadle JM.** Hypoxic enhancement of exosome release by breast cancer cells. *BMC Cancer* 12: 421, 2012.

27. **Koh YQ, Peiris HN, Vaswani K, Reed S, Rice GE, Salomon C, Mitchell MD.** Characterization of exosomal release in bovine endometrial intercaruncular stromal cells. *Reprod Biol Endocrinol* 14: 78, 2016.

28. **Kwon TH, Frøkiaer J, Fernández-Llama P, Knepper MA, Nielsen S.** Reduced abundance of aquaporins in rats with bilateral ischemia-induced acute renal failure: prevention by alpha-MSH. *Am J Physiol* 277: F413-F427, 1999.

29. **McCullough J, Clague MJ, Urbé S.** AMSH is an endosome-associated ubiquitin isopeptidase. *J Cell Biol* 166: 487-492, 2004.

30. **McDill BW, Li SZ, Kovach PA, Ding L, Chen F.** Congenital progressive hydronephrosis (cph) is caused by an S256L mutation in aquaporin-2 that affects its phosphorylation and apical membrane accumulation. *Proc Natl Acad Sci U S A* 103: 6952-6957, 2006.

31. **Mizuno E, Kobayashi K, Yamamoto A, Kitamura N, Komada M.** A deubiquitinating enzyme UBPY regulates the level of protein ubiquitination on endosomes. *Traffic* 7: 1017-1031, 2006.

32. **Moeller HB, Aroankins TS, Slengerik-Hansen J, Pisitkun T, Fenton RA.** Phosphorylation and ubiquitylation are opposing processes that regulate endocytosis of the water channel aquaporin-2. *J Cell Sci* 127: 3174-3183, 2014.

33. **Nielsen S, Frøkiaer J, Marples D, Kwon TH, Agre P, Knepper MA.** Aquaporins in the kidney: from molecules to medicine. *Physiol Rev* 82: 205-244, 2002.

34. **Oshikawa S, Sonoda H, Ikeda M.** Aquaporins in urinary extracellular vesicles (exosomes). *Int J Mol Sci* 17: pii: E957, 2016.

35. **Pagtalunan ME, Olson JL, Meyer TW.** Contribution of angiotensin II to late renal injury after acute ischemia. *J Am Soc Nephrol* 11: 1278-1286, 2000.

36. **Perucca J, Bouby N, Valeix P, Bankir L.** Sex difference in urine concentration across differing ages, sodium intake, and level of kidney disease. *Am J Physiol Regul Integr Comp Physiol* 292: R700-R705, 2007.

37. **Pisitkun T, Shen RF, Knepper MA.** Identification and proteomic profiling of exosomes in human urine. *Proc Natl Acad Sci U S A* 101: 13368-13373, 2004.

38. **Salomon C, Kobayashi M, Ashman K, Sobrevia L, Mitchell MD, Rice GE.** Hypoxia-induced changes in the bioactivity of cytotrophoblast-derived exosomes. *PLoS One* 8: e79636, 2013.

39. **Sharfuddin AA, Weisbord SD, Palevsky PM, Molitoris BA.** Acute kidney injury. In: *Brenner & Rector's The Kidney-10th ed*., edited by Skorecki K, Chertow, GM, Marsden PA, Taal MW, Yu ASL. Philadelphia, PA: Elsevier, 2016, p. 958-1011.

40. **Shimizu K, Sano M, Kita A, Sawai N, Iizuka-Kogo A, Kogo H, Aoki T, Takata K, Matsuzaki T.** Phosphorylation and dephosphorylation of aquaporin-2 at serine 269 and its subcellular distribution during vasopressin-induced exocytosis and subsequent endocytosis in the rat kidney. *Arch Histol Cytol* 77: 25-38, 2017.

41. **Sonoda H, Yokota-Ikeda N, Oshikawa S, Kanno Y, Yoshinaga K, Uchida K, Ueda Y, Kimiya K, Uezono S, Ueda A, Ito K, Ikeda M.** Decreased abundance of urinary exosomal aquaporin-1 in renal ischemia-reperfusion injury. *Am J Physiol Renal Physiol* 297: F1006-F1016, 2009.

42. **Takata K, Matsuzaki T, Tajika Y.** Aquaporins: water channel proteins of the cell membrane. *Prog Histochem Cytochem* 39: 1-83, 2004.

43. **van Balkom BW, van Raak M, Breton S, Pastor-Soler N, Bouley R, van der Sluijs P, Brown D, Deen PM.** Hypertonicity is involved in redirecting the aquaporin-2 water channel into the basolateral, instead of the apical, plasma membrane of renal epithelial cells. *J Biol Chem* 278: 1101-1107, 2003.

44. **Wen H, Frokiaer J, Kwon TH, Nielsen S.** Urinary excretion of aquaporin-2 in rat is mediated by a vasopressin-dependent apical pathway. *J Am Soc Nephrol* 10: 1416-1429, 1999.

45. **Xie L, Hoffert JD, Chou CL, Yu MJ, Pisitkun T, Knepper MA, Fenton RA.** Quantitative analysis of aquaporin-2 phosphorylation. *Am J Physiol Renal Physiol* 298: F1018-F1023, 2010.

46. **Yui N, Lu HA, Chen Y, Nomura N, Bouley R, Brown D.** Basolateral targeting and microtubule-dependent transcytosis of the aquaporin-2 water channel. *Am J Physiol Cell Physiol* 304: C38-C48, 2013.

47. **Zhang W, Zhou X, Zhang H, Yao Q, Liu Y, Dong Z.** Extracellular vesicles in diagnosis and therapy of kidney diseases. *Am J Physiol Renal Physiol* 311: F844-F851, 2016.

48. **Wang CJ, Grantham JJ, Wetmore JB.** The medicinal use of water in renal disease. *Kidney Int* 84: 45-53, 2013.

Fig. 1. Time course of changes in blood and urinary parameters in rats after renal bilateral ischemia/reperfusion (B-I/R).

Plasma urea nitrogen (A) and creatinine (B) concentrations, urine volume (C), and urinary osmolality (D) on days 3, 7, 21, and 35 are shown. Data are expressed as means ± SE. Numbers in parentheses indicate the number of animals tested. **P* <0.05 and ***P* <0.01, for comparison between the sham and B-I/R groups.

Fig. 2. Histological investigation of renal fibrosis after renal B-I/R.

A-D: Kidney sections were stained with Masson's trichrome on day 3 (A) in the sham group and on days 3 (B), 7 (C), and 35 (D) in the I/R group. Bars = 50 μm. g indicates glomerulus. E-F: Immunohistochemistry for α-SMA on day 3 (E) in the sham group and on days 3 (F), 7 (G & I), and 35 (H) in the I/R group. Black box in G indicates the region of high magnification in I. Brown staining indicates the presence of α-SMA. Bars = 50 μm.

Fig. 3. Urinary exosomal release of AQP1 after renal B-I/R.

A: Typical immunoblots of urinary exosomal AQP1 are shown. B: Immunoblotting results were quantified, and the summarized data are shown as a bar graph. Each value is expressed as a percentage of the mean value of urinary exosomal release of AQP1 in the sham group at each time point. Data are expressed as means ± SE. The numbers in parentheses indicate the numbers of animals tested. **P* <0.05 and ***P* <0.01, for comparison between the sham and I/R groups.

Fig. 4. Urinary exosomal release of AQP2 after renal B-I/R.

A: Typical immunoblots of urinary exosomal AQP2 are shown. B: Immunoblotting results were quantified and the summarized data are shown as a bar graph. Each value is expressed as a percentage of the mean value of urinary exosomal release of AQP2 in the sham group at each time point. Data are expressed as means ± SE. The numbers in parentheses indicate the numbers of animals tested. **P* <0.05 and ***P* <0.01, for comparison between the sham and I/R groups.

Fig. 5. Urinary exosomal release of Alix after renal B-I/R.

A: Typical immunoblots of urinary exosomal Alix are shown. B: Immunoblotting results were quantified and the summarized data are shown as a bar graph. Each value is expressed as a percentage of the mean value of urinary exosomal release of Alix in the sham group at each time

point. Data are expressed as means ± SE. The numbers in parentheses indicate the numbers of animals tested. **P <0.01, for comparison between the sham and I/R groups.

Fig. 6. Urinary exosomal release of TSG101 after renal B-I/R.

A: Typical immunoblots of urinary exosomal TSG101 are shown. B: Immunoblotting results were quantified and the summarized data are shown as a bar graph. Each value is expressed as a percentage of the mean value of urinary exosomal release of TSG101 in the sham group at each time point. Data are expressed as means ± SE. The numbers in parentheses indicate the numbers of animals tested. *P <0.05, and **P <0.01, for comparison between the sham and I/R groups.

Fig. 7. Renal expression of AQP1 after renal B-I/R.

A: Typical immunoblots of renal AQP1 are shown. B: Quantitative data were obtained from immunoblot analyses, and the summarized data after normalization to the corresponding level of β-actin are shown as a bar graph. Each value is expressed as a percentage of the mean level of renal expression of AQP1 in the sham group at each time point. Data are expressed as means ± SE. Numbers in parentheses indicate the numbers of animals tested. *P <0.05, and **P <0.01, for comparison between the sham and I/R groups.

Fig. 8. Renal expression of AQP2 after renal B-I/R.

A: Typical immunoblots of renal AQP2 are shown. B: Quantitative data were obtained from immunoblot analyses and the summarized data after normalization to the corresponding level of β-actin are shown as a bar graph. Each value is expressed as a percentage of the mean level of renal expression of AQP2 in the sham group at each time point. Data are expressed as means ± SE. Numbers in parentheses indicate the numbers of animals tested. *P <0.05, and **P <0.01, for comparison between the sham and I/R groups.

Fig. 9. Immunohistochemistry of renal AQP1 after renal B-I/R.

Kidney sections were stained with anti-AQP1 antibody on day 3 (A) in the sham group and on days 3 (B), 7 (C), and 35 (D) in the I/R group. Representative images of the cortex are shown. Brown staining indicates the presence of AQP1. Bars = 100 μm. g indicates glomerulus.

Fig. 10. Immunohistochemistry of renal AQP2 after renal B-I/R.

Kidney sections were stained with anti-AQP2 antibody on day 3 (A & B) in the sham group and on days 3 (C & D), 7 (E - G), and 35 (H & I) in the I/R group. Representative images of the medulla are shown. Black boxes in A, C, E, F, and H indicate the region of high magnification in B, D, F, G, and I, respectively. Brown staining indicates the presence of AQP2. Bars = 50 μm.

Fig. 11. Specificity of the anti-pS256 antibody demonstrated by immunohistochemistry.
A-C: To investigate the specificity of anti-S256-phosphorylated AQP2 antibody (pS256Ab), peptide preadsorption was performed on kidney sections (same sample as in ref 40) from an AVP-administered rat. One section was incubated with pS256Ab (A). One section was incubated with pS256Ab in the presence of the Ser256-phosphorylated antigen peptide (TM61) (B). One section was incubated with pS256Ab in the presence of the non-phosphorylated peptide (TM64) (C). Each photograph of the inner medulla was taken under the same conditions. Arrows indicate autofluorescence of erythrocytes. D-G: Paraffin sections of the kidney from an AVP-administered rat were treated with lambda protein phosphatase (F, G) or untreated (D, E) before immunolabeling to investigate the specificity of the pS256Ab. Sections were processed for double immunofluorescence labeling with pS256Ab (D & F) and goat AQP2Ab (E & G). Images of the inner medulla were taken under the same conditions for each primary antibody. Arrows indicate autofluorescence of erythrocytes. Bars = 100 μm.

Fig. 12. Urinary exosomal release of the S256-phosphorylated form of AQP2 after renal B-I/R.
A: Typical immunoblots of the S256-phosphorylated form of AQP2 are shown.
B: Immunoblotting results were quantified and the summarized data are shown as a bar graph. Each value is expressed as a percentage of the mean urinary exosomal release of S256-phosphorylated AQP2 in the sham group at each time point. Data are expressed as means ± SE. The numbers in parentheses indicate the numbers of animals tested. *P <0.05, for comparison between the sham and I/R groups. C: The relationship between urinary exosomal release of total AQP2 and S256-phosphorylated AQP2. The line is the least-squares regression line.

Fig. 13. Urinary exosomal release of the S269-phosphorylated form of AQP2 after renal B-I/R.

A: Typical immunoblots of the S269-phosphorylated form of AQP2 are shown. B: Immunoblotting results were quantified and the summarized data are shown as a bar graph. Each value is expressed as a percentage of the mean urinary exosomal release of S269-phosphorylated AQP2 in the sham group at each time point. Data are expressed as means ± SE. The numbers in parentheses indicate the numbers of animals tested. *P <0.05, for comparison between the sham and I/R groups. C: The relationship between urinary exosomal release of total AQP2 and S269-phosphorylated AQP2. The line is the least-squares regression line.

Fig. 14. Renal histology after unilateral ischemia/reperfusion (U-I/R).

A-D: Kidney sections were stained with Masson's trichrome on day 7 (A) in the sham group and on days 7 (B), and 35 (C) in the U-I/R group. Bars = 50 μm. g indicates glomerulus. E-F: Immunohistochemistry for α-SMA on day 7 (D) in the sham group and on days 7 (E) and 35 (F) in the U-I/R group. Bars = 100 μm. G-I: Immunohistochemistry for AQP1 on day 7 (G) in the sham group and on days 7 (H) and 35 (I) in the U-I/R group. Representative images of the cortex are shown. Bars = 100 μm. g indicates glomerulus. J-L: Immunohistochemistry for AQP2 on day 7 (G) in the sham group and on days 7 (H) and 35 (I) in the U-I/R group. Representative images of the medulla are shown. The smaller black box in K indicates the region of the bigger black box in K. Bars = 100 μm. g indicates glomerulus.

Fig. 15. Urinary exosomal release of AQP1, AQP2, Alix, and TSG101 after renal U-I/R.

Typical immunoblots of urinary exosomal AQP1 (A), AQP2 (C), Alix (E), and TSG101 (G), and the summarized data (B for AQP1; D for AQP2; F for Alix; H for TSG101) are shown. In each bar graph, each value is expressed as a percentage of the mean value in the sham group at each time point. Data are expressed as means ± SE. The numbers in parentheses indicate the numbers of animals tested. *P <0.05, for comparison between the sham and U-I/R groups.

761 **Table 1.** Changes in blood and urinary parameters after renal U-I/R.

	Group	day 3	day 7	day 35
Plasma creatinine (mg / dl)	sham	0.46 ± 0.03 (n = 8)	0.45 ± 0.04 (n = 8)	0.43 ± 0.02 (n = 4)
	U-I/R	4.09 ± 1.08 ** (n = 8)	2.04 ± 0.87** (n = 8)	0.50 ± 0.04 (n = 4)
Blood urea nitrogen (mg / dl)	sham	23.4 ± 1.4 (n = 8)	23.8 ± 1.5 (n = 8)	25.4 ± 0.5 (n = 4)
	U-I/R	157.3 ± 29.9** (n = 8)	87.8 ± 31.9** (n = 8)	29.0 ± 2.5 (n = 4)
Urine volume (ml)	sham	n.d.	11.5 ± 1.2 (n = 4)	10.5 ± 1.9 (n = 4)
	U-I/R	n.d.	15.9 ± 0.4* (n = 4)	18.9 ± 1.7* (n = 4)
Urinary osmolality (mOsm / kg H_2O)	sham	n.d.	608.3 ± 67.1 (n = 4)	755.3 ± 113.7 (n = 4)
	U-I/R	n.d.	362.0 ± 31.6* (n = 4)	590.0 ± 80.5 (n = 4)

762 Data are expressed as means ± SE. *P < 0.05 and **P < 0.01 vs. sham at each time point.

763 n.d. indicates not determined.

Figure 1

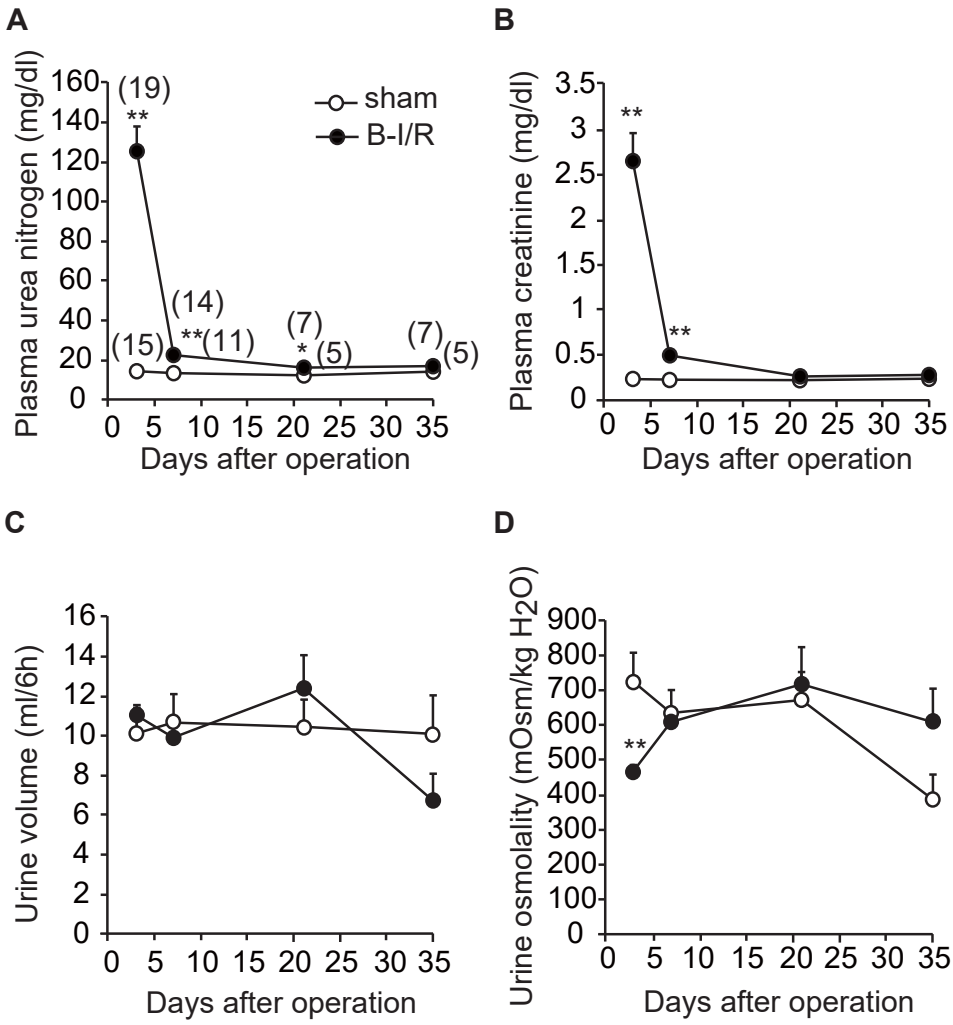
A
Plasma urea nitrogen (mg/dl)
160
140
120
100
80
60
40
20
0
(19)
**
(14)
**(11)
(7)
*
(5)
(7)
(5)
(15)
sham
B-I/R
0 5 10 15 20 25 30 35
Days after operation
B
Plasma creatinine (mg/dl)
3.5
3
2.5
2
1.5
1
0.5
0
**
**
0 5 10 15 20 25 30 35
Days after operation
C
Urine volume (ml/6h)
16
14
12
10
8
6
4
2
0
0 5 10 15 20 25 30 35
Days after operation
D
Urine osmolality (mOsm/kg H2O)
900
800
700
600
500
400
300
200
100
0
**
0 5 10 15 20 25 30 35
Days after operation

Figure 2

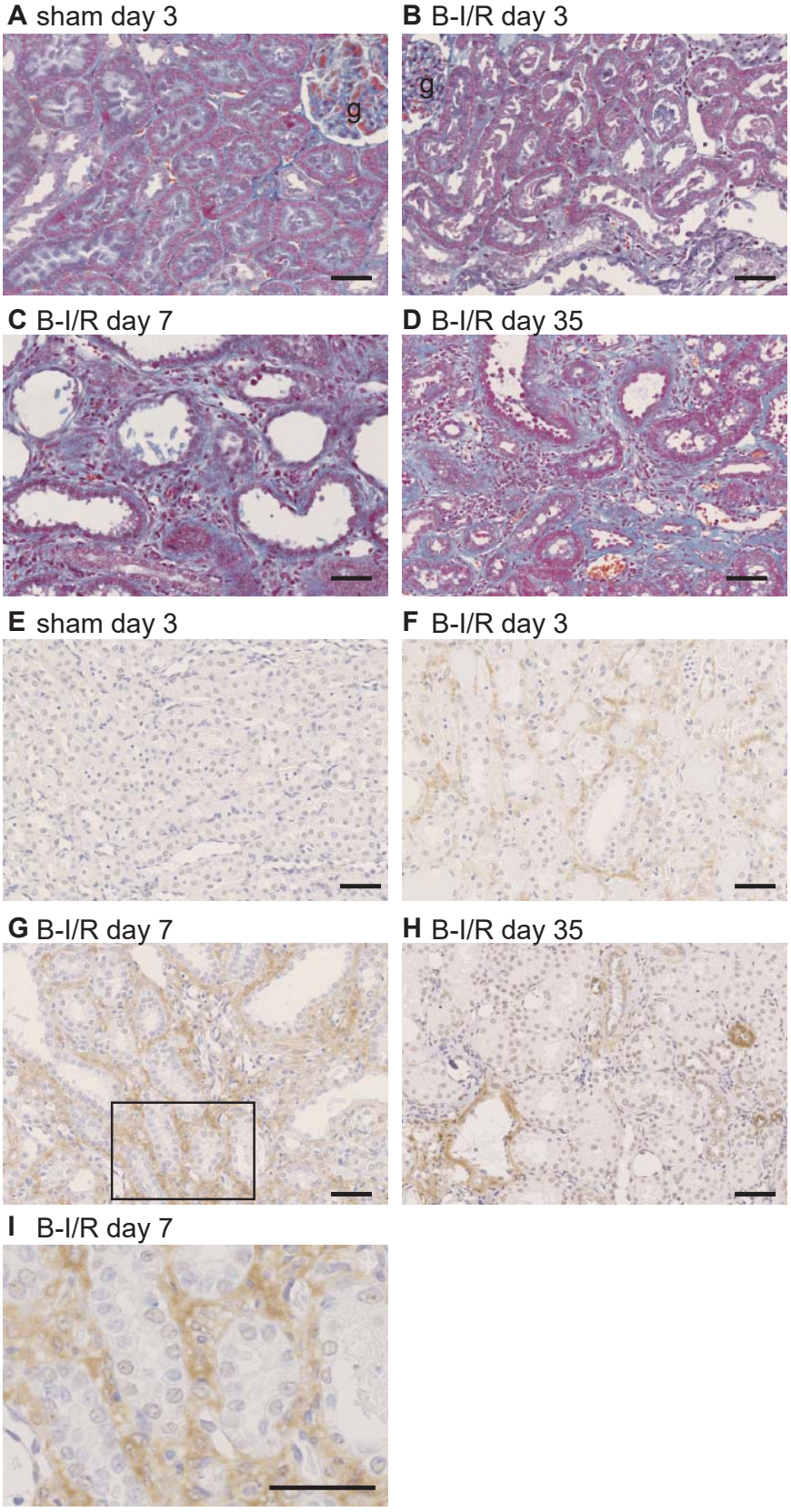
A sham day 3
g
B B-I/R day 3
g
C B-I/R day 7
D B-I/R day 35
E sham day 3
F B-I/R day 3
G B-I/R day 7
H B-I/R day 35
I B-I/R day 7

Figure 3

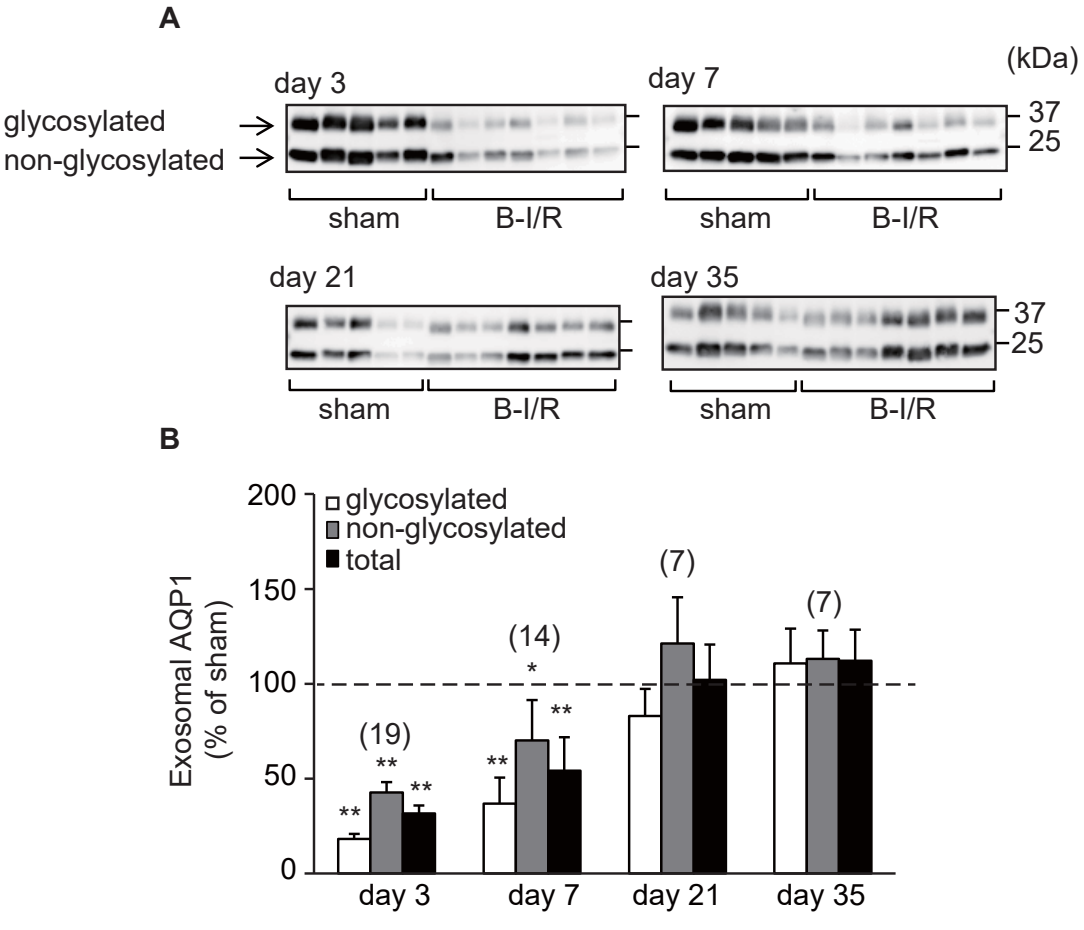
A
(kDa)
day 3
day 7
glycosylated
non-glycosylated
37
25
sham
B-I/R
sham
B-I/R
day 21
day 35
37
25
sham
B-I/R
sham
B-I/R
B
glycosylated
non-glycosylated
total
Exosomal AQP1
(% of sham)
200
150
100
50
0
(19)
(14)
(7)
(7)
*
**
**
**
**
**
day 3
day 7
day 21
day 35

Figure 4

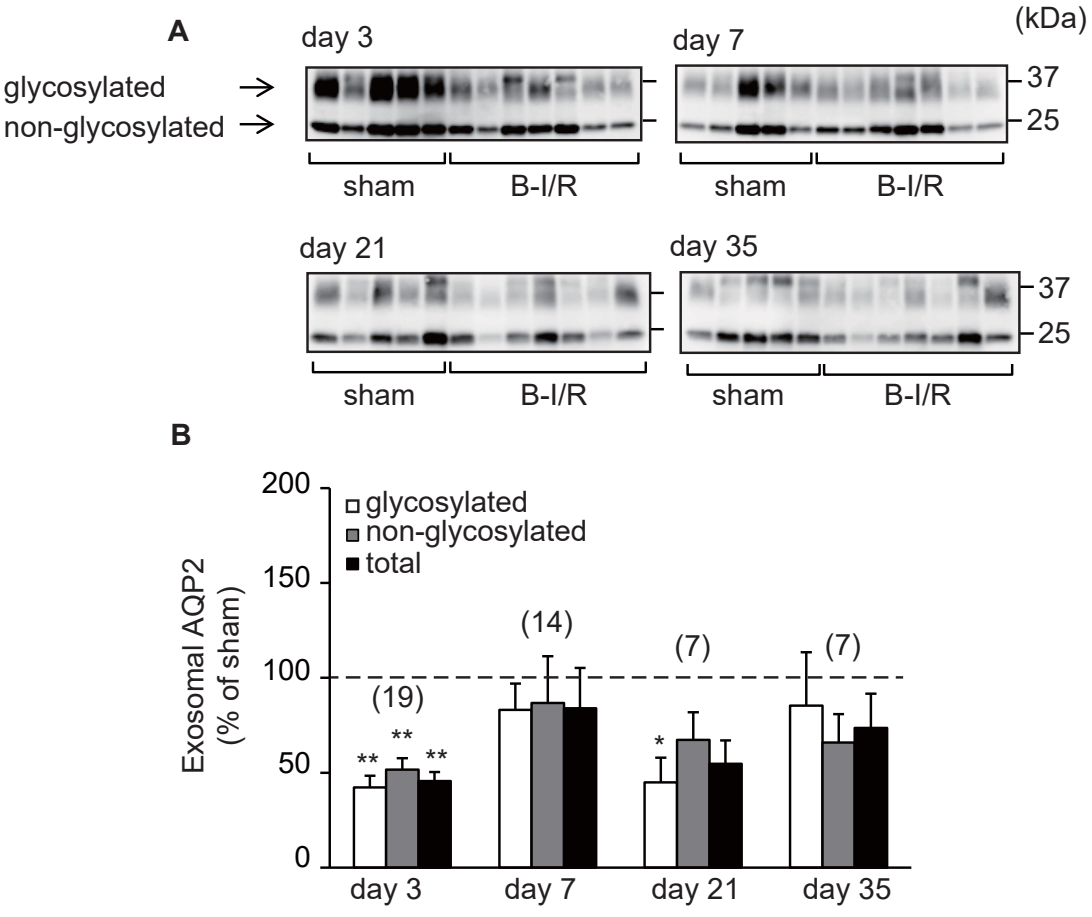
A
(kDa)
day 3
day 7
glycosylated
non-glycosylated
37
25
sham
B-I/R
sham
B-I/R
day 21
day 35
37
25
sham
B-I/R
sham
B-I/R
B
200
150
100
50
0
Exosomal AQP2
(% of sham)
glycosylated
non-glycosylated
total
(19)
(14)
(7)
(7)
**
**
**
*
day 3
day 7
day 21
day 35

Figure 5

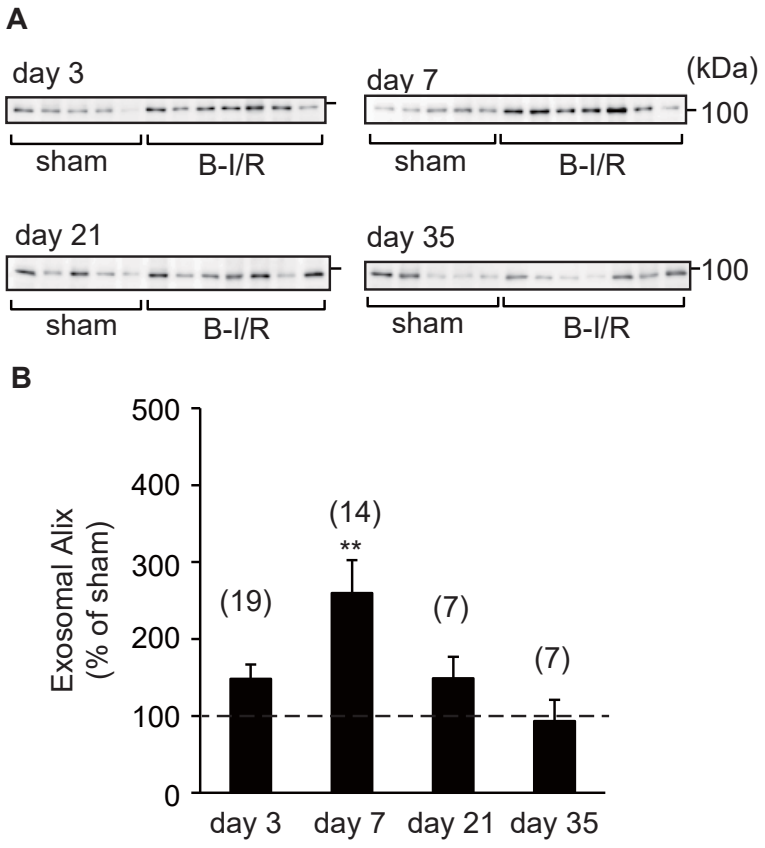
A
day 3
day 7
(kDa)
100
sham
B-I/R
sham
B-I/R
day 21
day 35
100
sham
B-I/R
sham
B-I/R
B
Exosomal Alix
(% of sham)
500
400
300
200
100
0
(19)
(14)
**
(7)
(7)
day 3
day 7
day 21
day 35

Figure 6

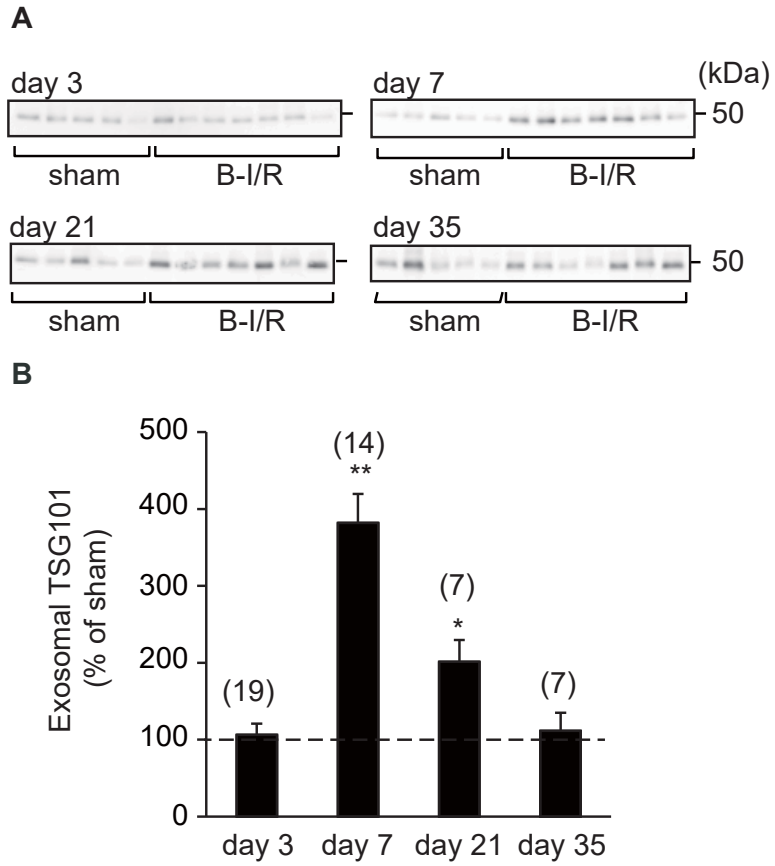
A
day 3
day 7
(kDa)
50
sham
B-I/R
sham
B-I/R
day 21
day 35
50
sham
B-I/R
sham
B-I/R
B
Exosomal TSG101
(% of sham)
500
400
300
200
100
0
(19)
(14)
**
(7)
*
(7)
day 3
day 7
day 21
day 35

Figure 7

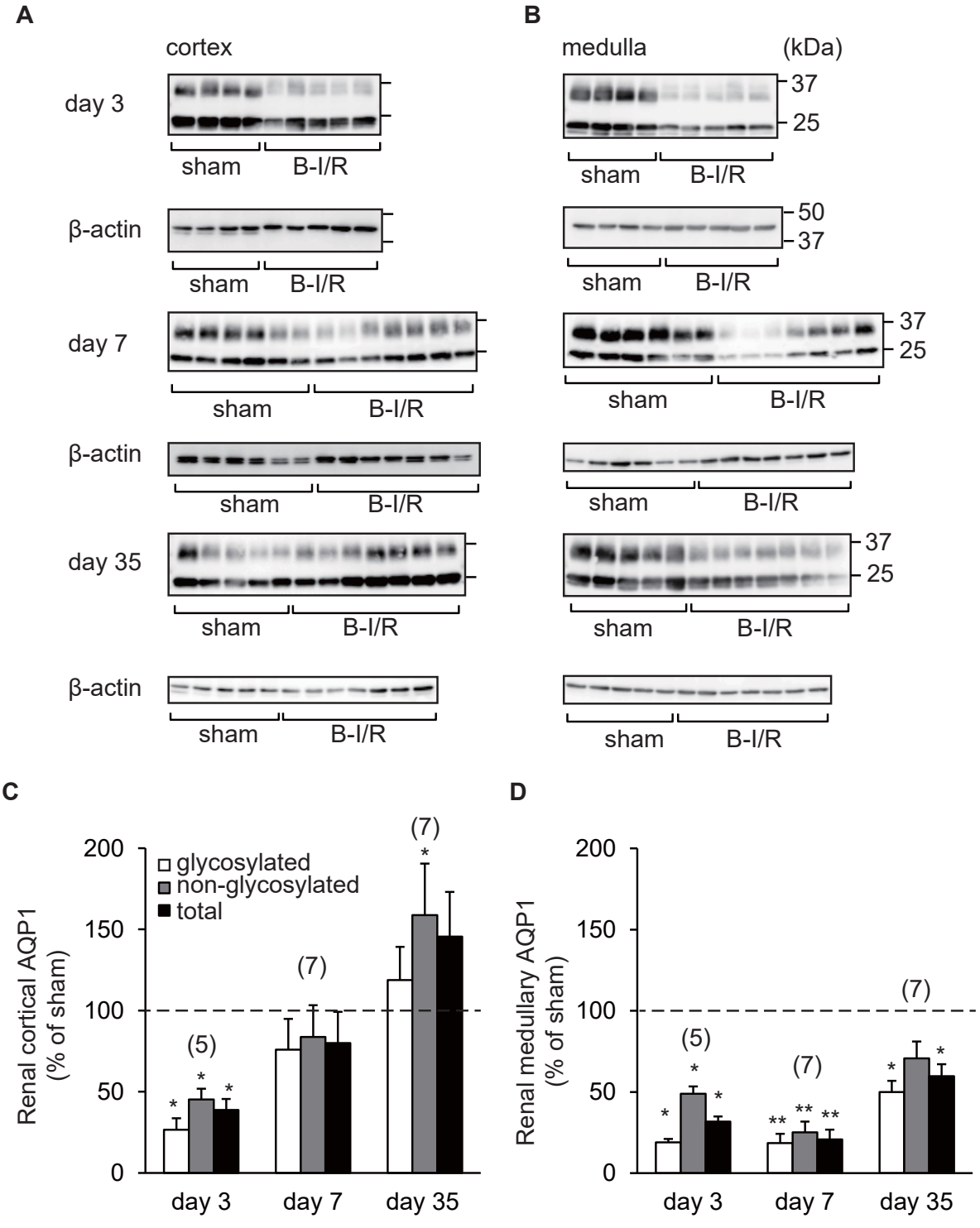
A
cortex
day 3
sham
B-I/R
β-actin
day 7
day 35
B
medulla
(kDa)
37
25
50
C
Renal cortical AQP1
(% of sham)
glycosylated
non-glycosylated
total
200
150
100
50
0
(5)
(7)
day 3
day 7
day 35
D
Renal medullary AQP1
(% of sham)

Figure 8

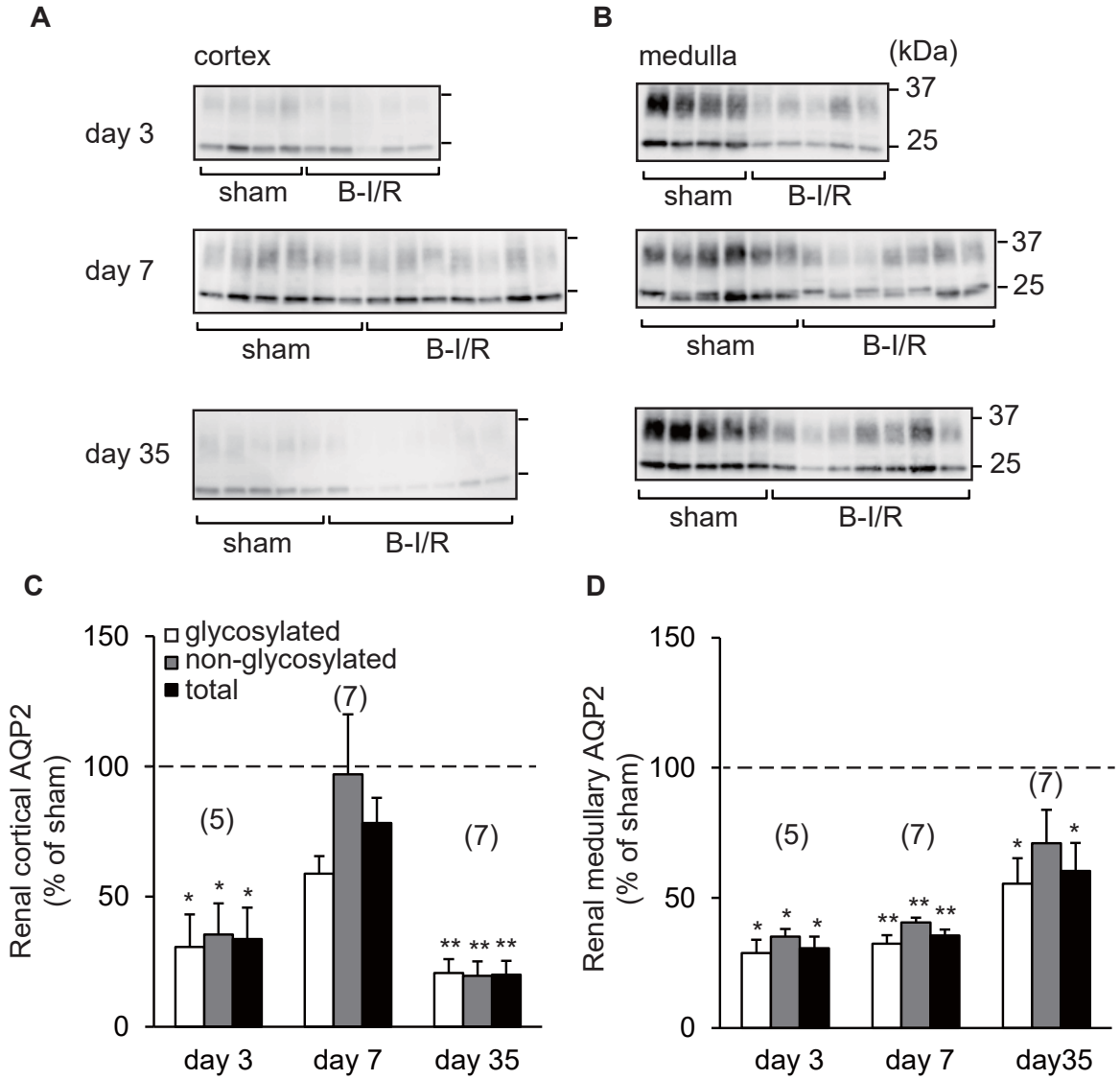
A
cortex
day 3
sham
B-I/R
day 7
sham
B-I/R
day 35
sham
B-I/R
B
medulla
(kDa)
37
25
sham
B-I/R
37
25
sham
B-I/R
37
25
sham
B-I/R
C
glycosylated
non-glycosylated
total
Renal cortical AQP2
(% of sham)
150
100
50
0
(5)
(7)
(7)
day 3
day 7
day 35
D
Renal medullary AQP2
(% of sham)
150
100
50
0
(5)
(7)
(7)
day 3
day 7
day35

Figure 9

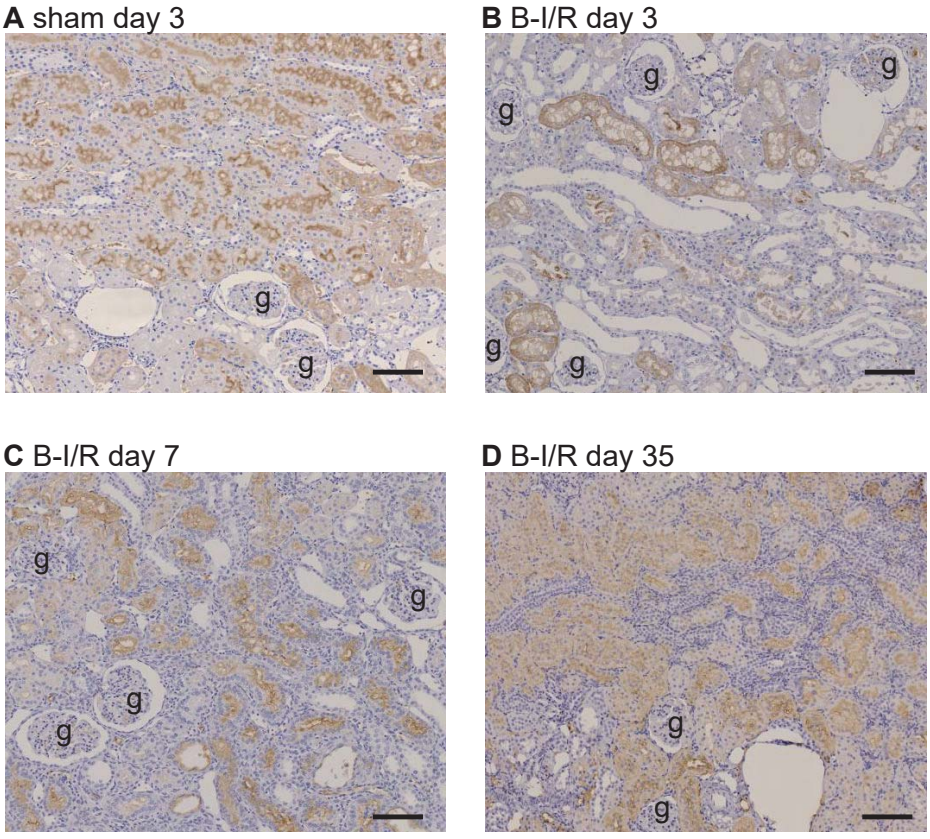

Figure 10

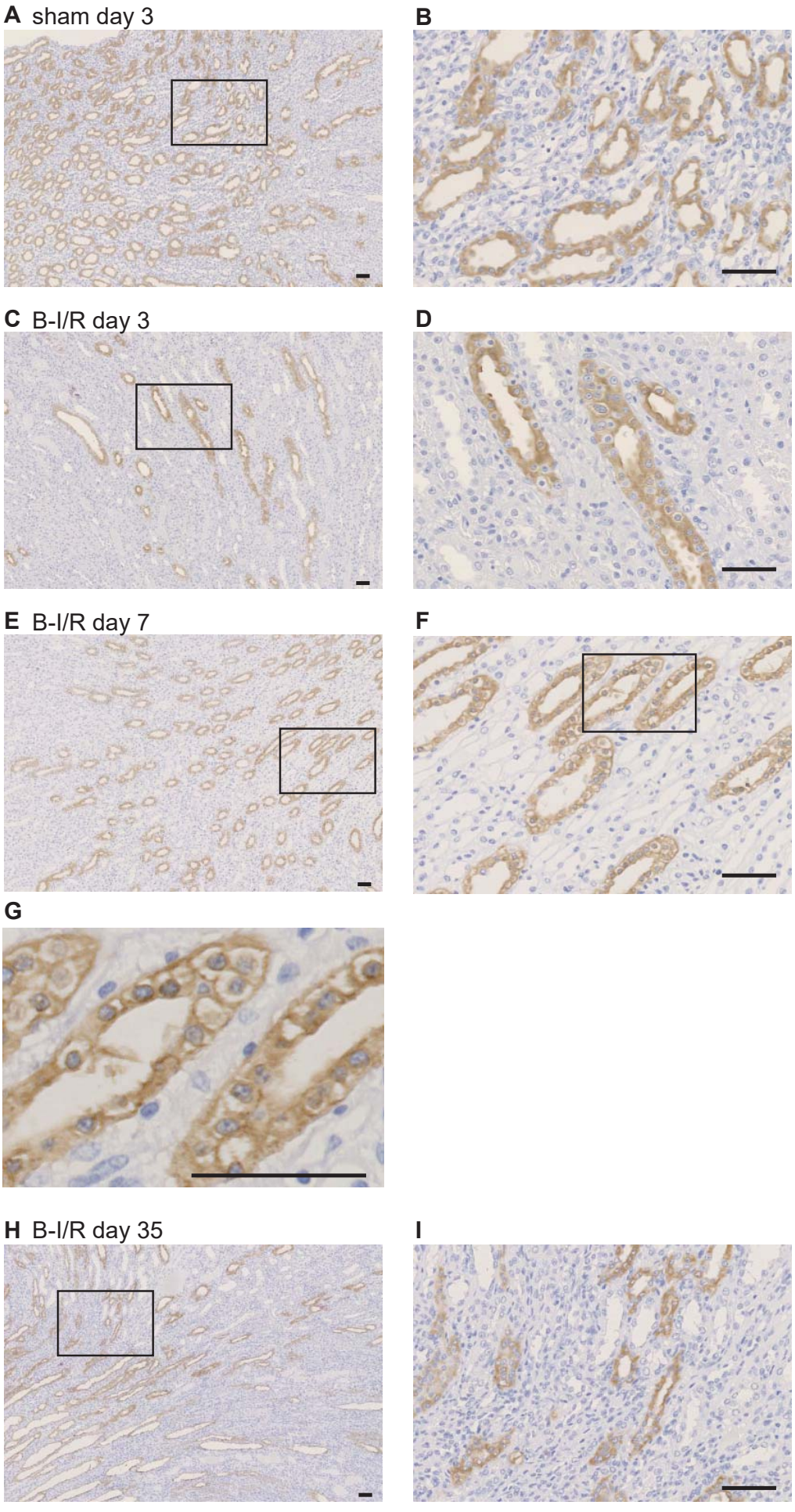

Figure 11

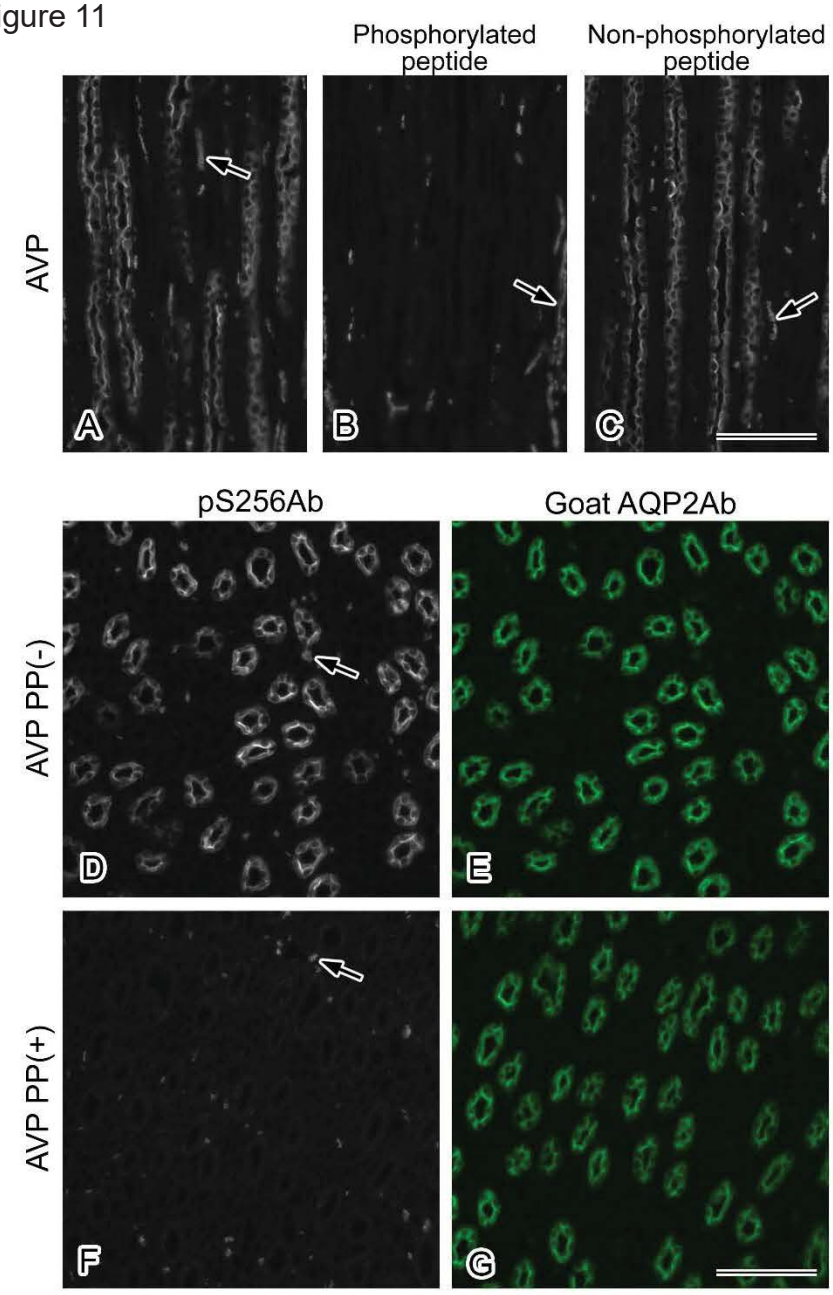
Phosphorylated peptide
Non-phosphorylated peptide
AVP
A
B
C
pS256Ab
Goat AQP2Ab
AVP PP(-)
D
E
AVP PP(+)
F
G

Figure 12

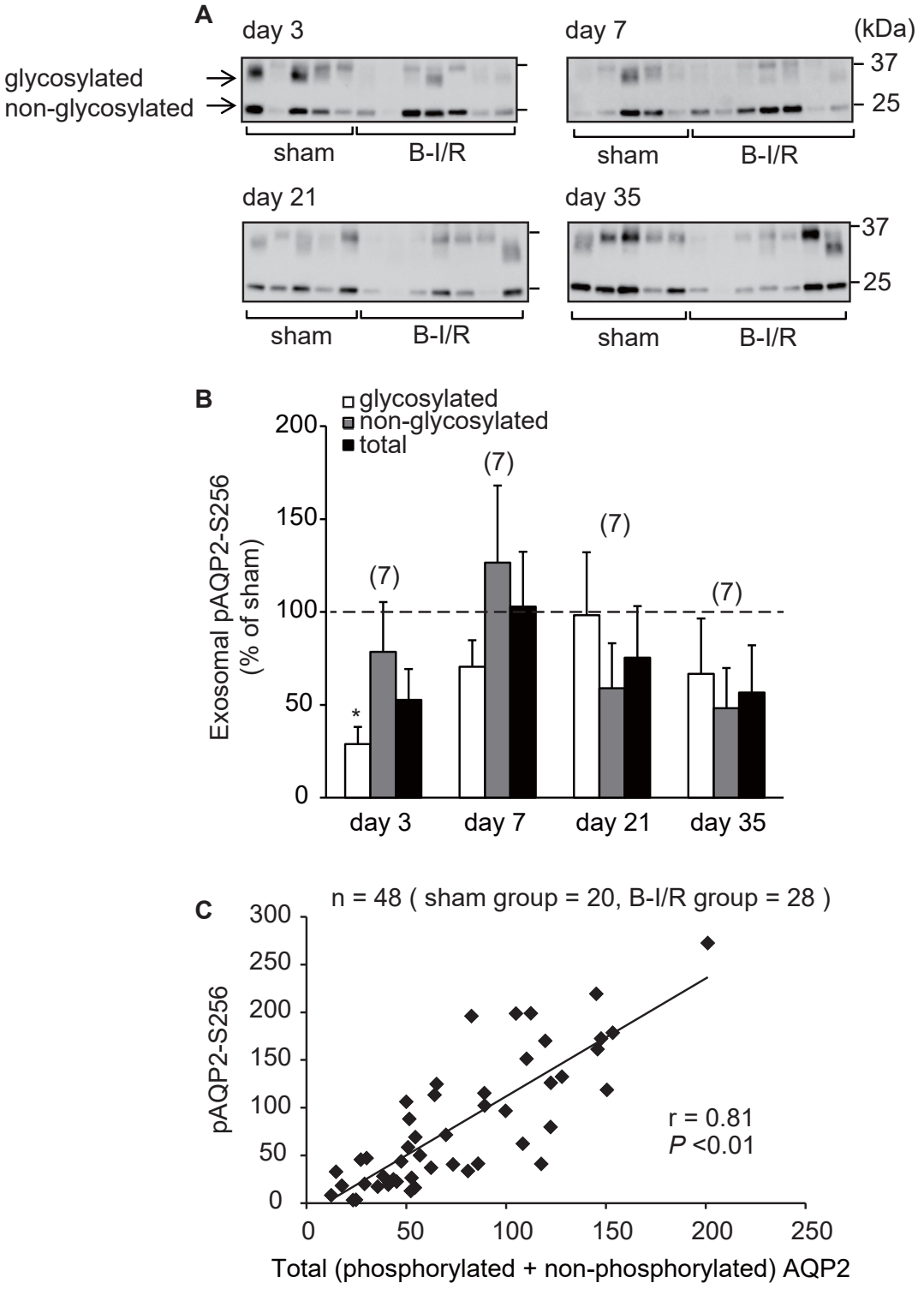
A
day 3
day 7
(kDa)
glycosylated
non-glycosylated
37
25
sham
B-I/R
day 21
day 35
B
glycosylated
non-glycosylated
total
Exosomal pAQP2-S256
(% of sham)
200
150
100
50
0
(7)
*
day 3
day 7
day 21
day 35
C
n = 48 (sham group = 20, B-I/R group = 28)
pAQP2-S256
300
250
200
150
100
50
0
r = 0.81
P <0.01
Total (phosphorylated + non-phosphorylated) AQP2

Figure 13

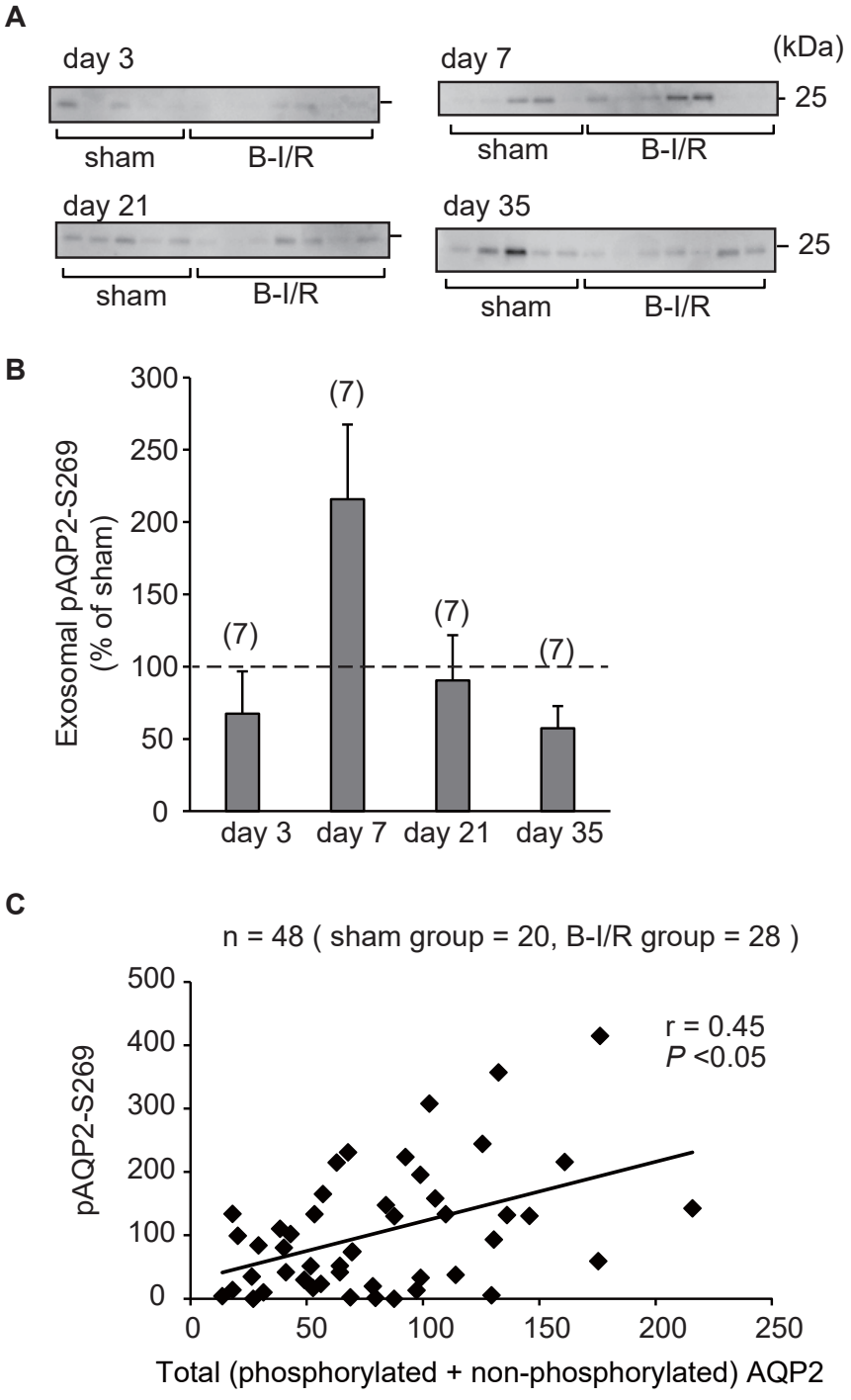
A
day 3
day 7
(kDa)
25
sham
B-I/R
day 21
day 35
25
B
Exosomal pAQP2-S269
(% of sham)
300
250
200
150
100
50
0
(7)
(7)
(7)
(7)
day 3
day 7
day 21
day 35
C
n = 48 (sham group = 20, B-I/R group = 28)
pAQP2-S269
500
400
300
200
100
0
r = 0.45
P <0.05
0
50
100
150
200
250
Total (phosphorylated + non-phosphorylated) AQP2

Figure 14

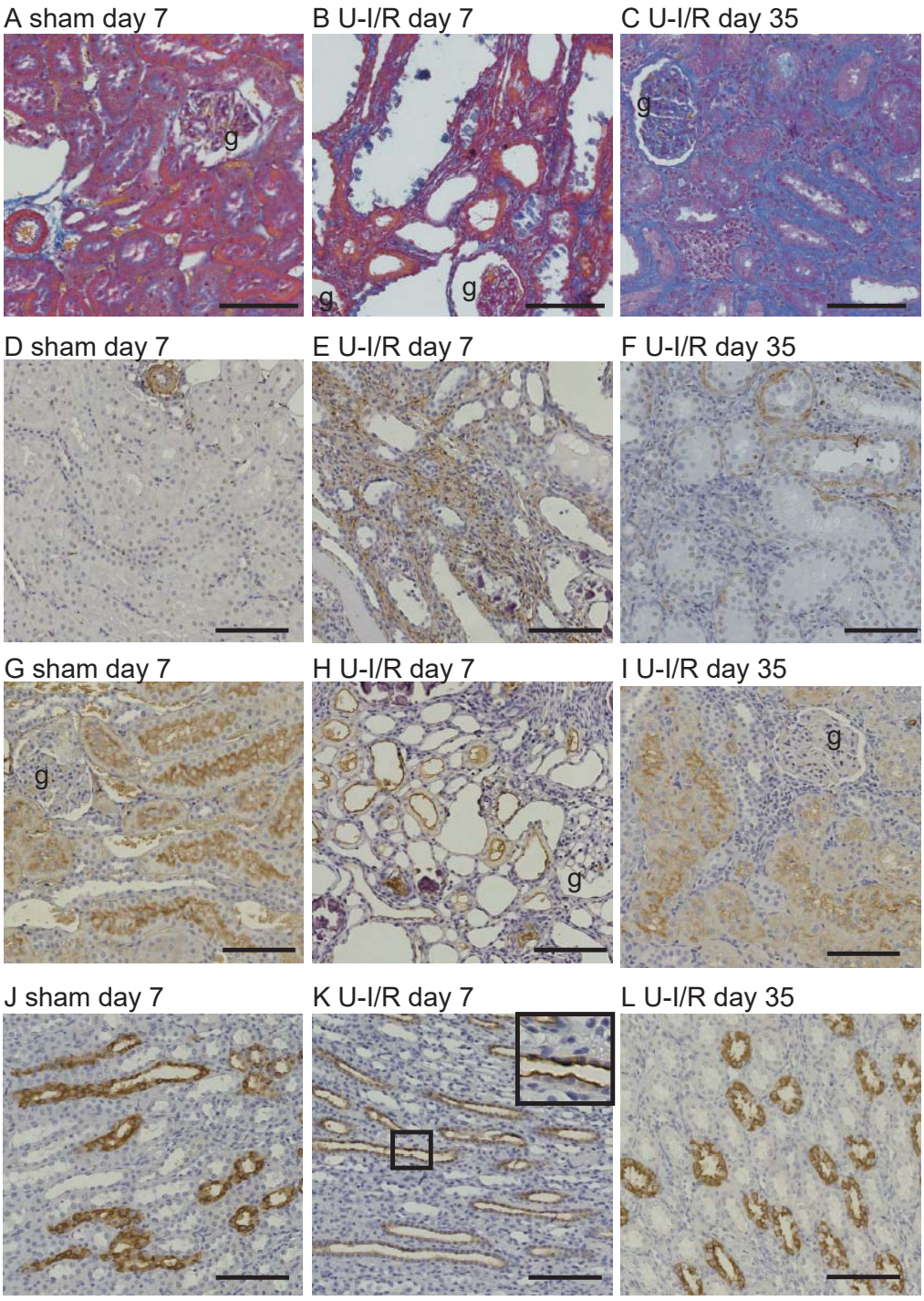
A sham day 7
B U-I/R day 7
C U-I/R day 35
D sham day 7
E U-I/R day 7
F U-I/R day 35
G sham day 7
H U-I/R day 7
I U-I/R day 35
J sham day 7
K U-I/R day 7
L U-I/R day 35
g

Figure 15

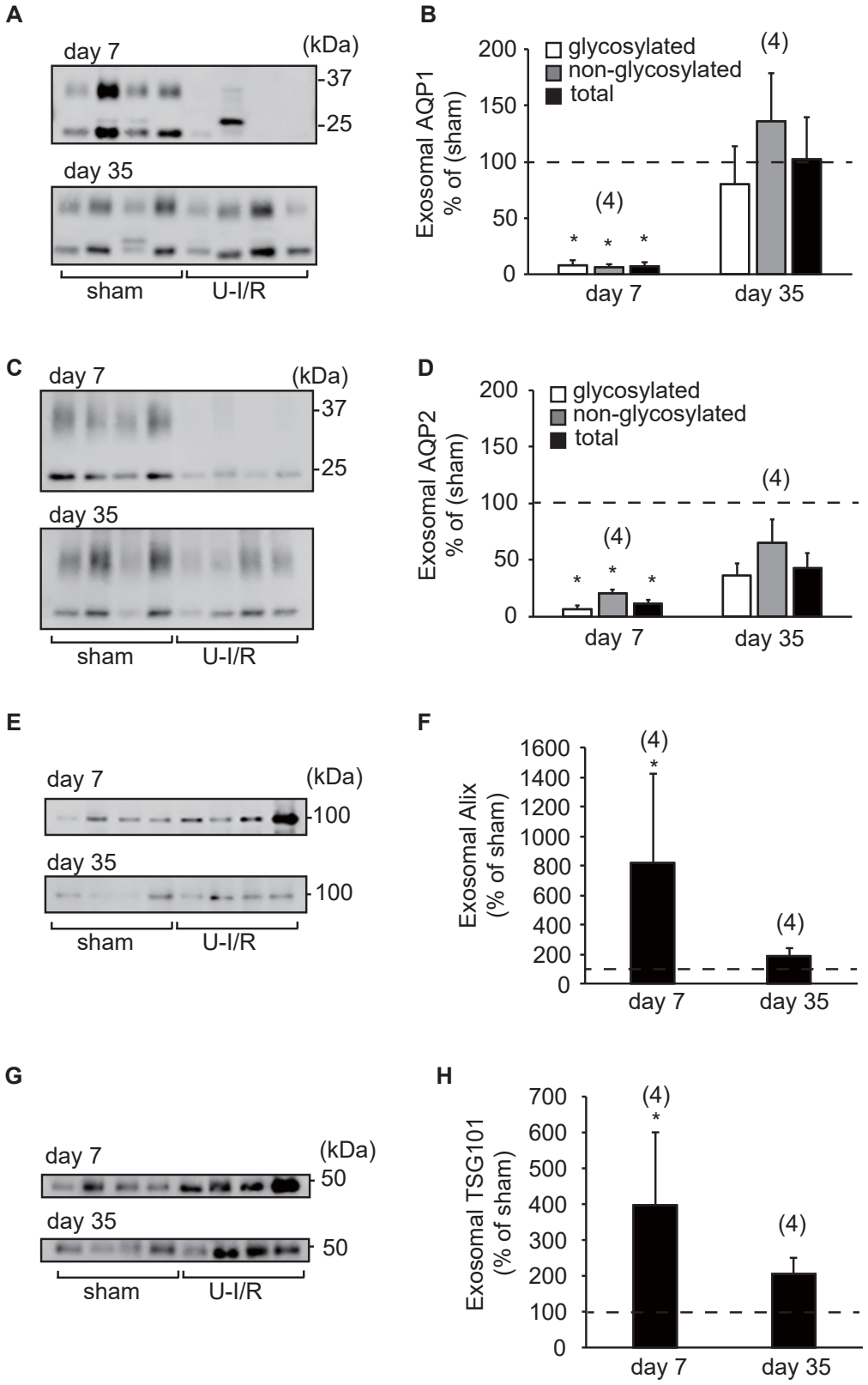
A
day 7
(kDa)
37
25
day 35
sham
U-I/R
B
glycosylated
non-glycosylated
total
Exosomal AQP1
% of (sham)
200
150
100
50
0
(4)
(4)
*
*
*
day 7
day 35
C
day 7
(kDa)
37
25
day 35
sham
U-I/R
D
glycosylated
non-glycosylated
total
Exosomal AQP2
% of (sham)
200
150
100
50
0
(4)
(4)
*
*
*
day 7
day 35
E
day 7
(kDa)
100
day 35
100
sham
U-I/R
F
Exosomal Alix
(% of sham)
1600
1400
1200
1000
800
600
400
200
0
(4)
*
(4)
day 7
day 35
G
day 7
(kDa)
50
day 35
50
sham
U-I/R
H
Exosomal TSG101
(% of sham)
700
600
500
400
300
200
100
0
(4)
*
(4)
day 7
day 35